

Review

# CO<sub>2</sub>-Selective Capture from Light Hydrocarbon Mixtures by Metal-Organic Frameworks: A Review

Hengcong Huang, Luyao Wang, Xiaoyu Zhang, Hongshuo Zhao and Yifan Gu \*

College of Environmental Science and Engineering, State Key Laboratory of Pollution Control and Resource Reuse, Tongji University, Siping Rd 1239, Shanghai 200092, China

\* Correspondence: 159219yifan\_gu@tongji.edu.cn

**Abstract:** CO<sub>2</sub> represents a typical impurity in light hydrocarbon feedstocks, which affects the quality of subsequent chemical products. Owing to their highly similar nature, industrial separation requires large amounts of energy. Adsorptive gas separation based on porous materials is considered an efficient alternative, as it can offer faster kinetics, higher selectivity, long-term stability and more energy-efficient regeneration. For the adsorption separation method, preferential CO<sub>2</sub> capture from gas mixtures in one step is more energy-efficient for direct purification than light hydrocarbons, saving about 40% energy by eliminating energy-intensive post-regeneration processes such as counter-current vacuum blowdown. Therefore, CO<sub>2</sub>-selective adsorbents are more sought-after than light hydrocarbon-selective adsorbents. Metal-organic frameworks (MOFs) have been demonstrated as outstanding physisorbents for CO<sub>2</sub> capture due to their configurable channels for CO<sub>2</sub> recognition, structural flexibility and large specific surface area. Many highly selective CO<sub>2</sub> adsorption behaviors of MOFs have been reportedly achieved by precise modulation of pore size, pore chemistry or structural flexibility. In this review, we discuss the emerging development of MOFs for CO<sub>2</sub>-selective capture from different light hydrocarbon mixtures. The challenges of CO<sub>2</sub> recognition and the strategies employed to achieve CO<sub>2</sub> selectivity over light hydrocarbon mixtures by MOFs are summarized. In addition, the current challenges and prospects in the field of MOFs for CO<sub>2</sub> capture are discussed and elaborated.

**Keywords:** CO<sub>2</sub> capture; metal-organic frameworks; light hydrocarbons; adsorption; separation



**Citation:** Huang, H.; Wang, L.; Zhang, X.; Zhao, H.; Gu, Y. CO<sub>2</sub>-Selective Capture from Light Hydrocarbon Mixtures by Metal-Organic Frameworks: A Review. *Clean Technol.* **2023**, *5*, 1–24. <https://doi.org/10.3390/cleantechnol5010001>

Academic Editor: Patricia Luis

Received: 18 October 2022

Revised: 12 December 2022

Accepted: 19 December 2022

Published: 20 December 2022



**Copyright:** © 2022 by the authors. Licensee MDPI, Basel, Switzerland. This article is an open access article distributed under the terms and conditions of the Creative Commons Attribution (CC BY) license (<https://creativecommons.org/licenses/by/4.0/>).

## 1. Introduction

Carbon dioxide (CO<sub>2</sub>) is a critical cause of global warming, which is a widespread public concern [1,2]. Global annual CO<sub>2</sub> emissions increased by approximately 130% between 1970 and 2020 and are expected to increase to 48–55 Gt/year by 2050 without intervention [3,4]. Therefore, carbon capture, utilization and storage have been considered key strategies by policymakers and oil companies, of which CO<sub>2</sub> capture is the core issue [5–7]. In the chemical industry, CO<sub>2</sub> is often formed as an impurity during the production of light hydrocarbons. For instance, natural gas or biogas (CH<sub>4</sub>) usually contains 5–70% carbon dioxide, which needs to be reduced to less than 2% for pipeline transportation and 50 ppm for liquefied natural gas [8,9]. Acetylene (C<sub>2</sub>H<sub>2</sub>) is typically produced by partial combustion of CH<sub>4</sub> or hydrocarbon cracking, which generally results in several gaseous impurities such as CH<sub>4</sub> and CO<sub>2</sub> [10]. The presence of CO<sub>2</sub> in light hydrocarbons affects the quality of subsequent chemical products, and it is challenging to trap CO<sub>2</sub> from their mixture due to their highly similar physical properties (Table 1) [11]. Absorption with aqueous amine and cryogenic distillation are traditionally used for CO<sub>2</sub> capture and light hydrocarbon purification, but these methods suffer from large amounts of waste streams and high regeneration energy consumption [12–14]. Comparatively, adsorptive gas separation based on porous adsorbents in hydrocarbon purification is considered more energy-efficient, as it can offer faster kinetics, higher selectivity and more energy-efficient

regeneration [5,15–18]. The adsorption separation process is performed by introducing a gas mixture into a column filled with porous materials, adsorbing the strongly adsorbed components and obtaining the outlet weakly adsorbed components; the strongly adsorbed components are subsequently recovered in the desorption process. However, the desorption process involves energy-intensive steps such as countercurrent evacuation [19–21]. It is estimated to cost approximately 40% more energy to harvest high-purity products through the desorption process than to collect the weakly adsorbed gas product directly at the outlet [22,23]. Therefore, porous materials for CO<sub>2</sub>-selective adsorption are more sought-after than hydrocarbon-selective materials, as hydrocarbons are the target products in practical applications. Direct CO<sub>2</sub> capture from light hydrocarbon mixtures is more energy-efficient and effective.

**Table 1.** Main physicochemical properties of CO<sub>2</sub> and common light hydrocarbons [24,25].

Property	CO <sub>2</sub>	CH <sub>4</sub>	C <sub>2</sub> H <sub>2</sub>	C <sub>2</sub> H <sub>4</sub>	C <sub>2</sub> H <sub>6</sub>
Kinetic diameter (Å)	3.30	3.76	3.30	4.16	4.44
Boiling point (K)	194.7	111.6	189.3	169.4	184.5
Polarizability ( $\times 10^{-25}$ cm <sup>3</sup> )	29.11	26.0	33.3–39.3	42.52	44.3–44.7
Quadrupole moment ( $\times 10^{26}$ esu cm <sup>2</sup> )	−4.30	0	7.50	1.5	0.65

The development of porous materials has explosively grown in the last few decades, the most promising of which are metal-organic frameworks (MOFs), also referred to as porous coordination polymers (PCPs). MOFs assembled from organic linkers and metal cluster based secondary building units (SBUs) generally possess high surface areas and easily controlled pore sizes and environments, with infinite possibilities. MOFs have been demonstrated as outstanding physisorbents for CO<sub>2</sub> capture due to their highly configurable channels for CO<sub>2</sub> molecular recognition (Figure 1) [24,26–32]. Therefore, a detailed update on the current status of MOFs with CO<sub>2</sub> selectivity for CO<sub>2</sub>/light hydrocarbon separation is urgently needed and would provide insight into their future development. Through this review, we aim to discuss the advancement of MOFs for the selective capture of CO<sub>2</sub> from different light hydrocarbon mixtures (CO<sub>2</sub>/CH<sub>4</sub>, CO<sub>2</sub>/C<sub>2</sub>H<sub>2</sub>, CO<sub>2</sub>/C<sub>2</sub>H<sub>4</sub>, etc.) in one-step purification of light hydrocarbons. As a departure from other reviews, we focus on evaluating MOFs with CO<sub>2</sub> selectivity. Herein, we describe the challenges of CO<sub>2</sub>-selective recognition and summarize the strategies adopted to achieve CO<sub>2</sub> selectivity. Furthermore, we discuss the current challenges and prospects in the field of MOFs for CO<sub>2</sub> capture.

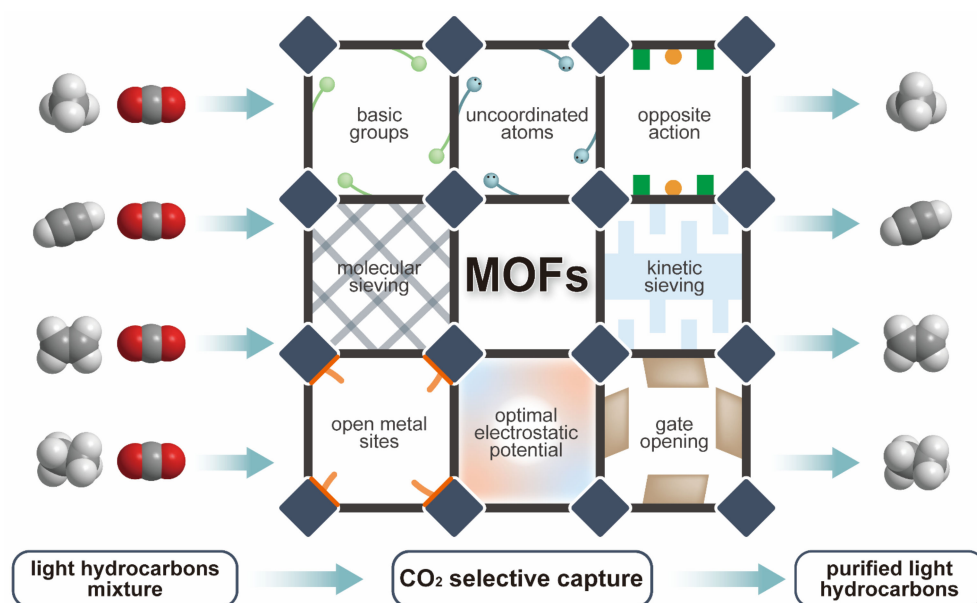


**Figure 1.** Schematic diagram of the process and typical strategies of CO<sub>2</sub>-selective capture from light hydrocarbon mixtures by metal-organic frameworks.

## 2. CO<sub>2</sub>-Selective Capture from CO<sub>2</sub>/CH<sub>4</sub> Mixture

Natural gas, the main component of which is CH<sub>4</sub>, is a clean energy source and a feedstock for bulk chemicals, for which the CO<sub>2</sub> concentration is required to be less than 2% for pipeline transportation and 50 ppm for liquefied natural gas [8,9]. Therefore, the separation of the CO<sub>2</sub>/CH<sub>4</sub> mixture is an essential process for the industrial utilization of natural gas. However, CO<sub>2</sub> and CH<sub>4</sub> exhibit close polarizability (CH<sub>4</sub>,  $26.0 \times 10^{-25} \text{ cm}^3$ ; CO<sub>2</sub>,  $29.11 \times 10^{-25} \text{ cm}^3$ ) and kinetic diameters (CH<sub>4</sub>, 3.76 Å; CO<sub>2</sub>, 3.30 Å). By exploiting the slight differences in molecular size and polarizability, there are two solutions available using MOFs to trap CO<sub>2</sub> from CO<sub>2</sub>/CH<sub>4</sub>: (1) modulating the pore size/shape of MOFs for kinetic separation or molecular sieving and (2) constructing functional sites with enhanced CO<sub>2</sub> interactions, such as open metal sites (OMSs), quadrupole interaction sites, hydrogen bonding sites, Lewis basic sites, van der Waals interaction sites, etc. (Table 2).

**Table 2.** Representative MOFs for CO<sub>2</sub>-selective capture from CO<sub>2</sub>/CH<sub>4</sub> mixtures \*.

MOF	Functional Site	CO <sub>2</sub> Capacity (mmol/g)	CO <sub>2</sub> /CH <sub>4</sub> Selectivity	Q <sub>st</sub> for CO <sub>2</sub> (kJ/mol)	Ref.
MOF-508b	quadrupole interactions	1.78 <sup>a</sup>	3–6 <sup>a</sup>	14.9	[33,34]
ZIF-78	Dipole–quadrupole interactions	2.32	10.6 <sup>b</sup>	—	[35]
Mg-MOF-74	open metal sites	8.61	8	73	[36]
MAF-66	uncoordinated N atoms	4.41	5.8	26	[37]
SIFSIX-1-Cu	SiF <sub>6</sub> <sup>2-</sup>	5.2	10.5	27	[38]
SIFSIX-2-Cu-i	SiF <sub>6</sub> <sup>2-</sup>	5.4	33	31.9	[39]
SIFSIX-3-Zn	SiF <sub>6</sub> <sup>2-</sup>	2.54	231	45	[39]
SYSU	narrow channels	3.11	4.7	28.2	[40]
NJU-Bai7	narrow channels	2.91	14.1 <sup>c</sup>	40.5	[40]
NJU-Bai8	uncoordinated N atoms	2.57	40.8 <sup>c</sup>	37.7	[40]
PEI-incorporated amine-MIL-101(Cr)	amine groups	3.6	931	—	[41]
Qc-5-Cu-sql-β	molecular sieving	2.16 <sup>d</sup>	3300	36	[42]
SIFSIX-14-Cu-i	molecular sieving	4.71	46.7 <sup>e</sup>	37.7	[43]
NJU-Bai35	molecular sieving	3.125	11.6	33.37	[44]
dptz-CuTiF <sub>6</sub>	TiF <sub>6</sub> <sup>2-</sup>	4.52	—	33.3	[28]
dptz-CuSiF <sub>6</sub>	SiF <sub>6</sub> <sup>2-</sup>	4.04	—	38.2	[28]

Table 2. Cont.

MOF	Functional Site	CO <sub>2</sub> Capacity (mmol/g)	CO <sub>2</sub> /CH <sub>4</sub> Selectivity	Q <sub>st</sub> for CO <sub>2</sub> (kJ/mol)	Ref.
TIFSIX-3-Ni	TiF <sub>6</sub> <sup>2-</sup>	2.213	158	50.0	[45]
NbOFFIVE-1-Ni	NbOF <sub>5</sub> <sup>2-</sup>	2.308	366	54.0	[45]
TIFSIX-2-Cu-i	TiF <sub>6</sub> <sup>2-</sup>	4.229	16	35.8	[45]
ZU-66	molecular sieving	4.56	136	35	[46]
IRH-3	uncoordinated N atoms	2.7	27	—	[47]
In(aip) <sub>2</sub>	molecular sieving and -NH <sub>2</sub> groups	1.27	1808	34.3	[48]
UTSA-280	molecular sieving	3.00	molecular sieving	42.9	[49]
UiO-66(N <sub>10%</sub> -Zr)	uncoordinated N atoms and kinetic effect	2.1	326	35.7	[50]
MUF-16	N-H...O and C-H...O	2.13 <sup>d</sup>	6690 <sup>d</sup>	32.3	[51]
MUF-16 (Mn)	N-H...O and C-H...O	2.25 <sup>d</sup>	470 <sup>d</sup>	36.6	[51]
MUF-16 (Ni)	N-H...O and C-H...O	2.13 <sup>d</sup>	1220 <sup>d</sup>	37.3	[51]
Cu-F-pymo	molecular sieving	1.61 <sup>f</sup>	>10 <sup>7</sup>	29.1	[52]
[Cu <sub>3</sub> (μ <sub>3</sub> -OH)(PCA) <sub>3</sub> ]	open metal sites	2.93	15.9	31.5	[53]
[Zn(odip) <sub>0.5</sub> (bpe) <sub>0.5</sub> ]	gate opening	5.3	376.0	42.3	[54]

\* Unless otherwise specified, the capacity data were all recorded at 1 bar, 298 K; CO<sub>2</sub>/CH<sub>4</sub> selectivity is the ideal adsorbed solution theory (IAST) selectivity for 50/50 (v/v) CO<sub>2</sub>/CH<sub>4</sub> mixtures at 1 bar, 298 K; Q<sub>st</sub> for CO<sub>2</sub> is the value at zero coverage; “—” indicates that data were not found; <sup>a</sup> at 303 K; <sup>b</sup> Henry’s Law selectivity; <sup>c</sup> separation ratios at 273 K; <sup>d</sup> at 293 K; <sup>e</sup> calculated by the uptake ratio of CO<sub>2</sub>/CH<sub>4</sub> at 1 bar; <sup>f</sup> calculated by (volumetric uptake)/(crystal density).

Bastin et al. presented the first example of the removal of CO<sub>2</sub> from a binary CO<sub>2</sub>/CH<sub>4</sub> mixture by MOFs [33,34]. MOF-508 showed CO<sub>2</sub> uptake of 1.78 mmol/g and moderate selectivity in the range of 3–6 at 303 K, 1 bar. The very low adsorption enthalpy of 14.9 kJ/mol for CO<sub>2</sub> and 5.1 kJ/mol for CH<sub>4</sub> suggested that the CO<sub>2</sub> interaction with MOF-508 probably originated from quadrupole interaction and/or van der Waals interaction.

Due to the slight differences in molecular size between CO<sub>2</sub> and CH<sub>4</sub>, some rigid MOF materials with molecular sieving effects achieved CO<sub>2</sub> capture from CO<sub>2</sub>/CH<sub>4</sub> with high selectivity by reducing the aperture of MOFs so that only smaller CO<sub>2</sub> could diffuse into the pores, whereas larger CH<sub>4</sub> was completely excluded.

UTSA-280 is a typical rigid MOF with a molecular sieving effect [49,55]. The cross-sectional area of its 1D channel is approximately 14.4 Å<sup>2</sup>, which is smaller than that of CH<sub>4</sub> (minimum: 15.1 Å<sup>2</sup>) but larger than that of CO<sub>2</sub> (minimum: 10.7 Å<sup>2</sup>). The CO<sub>2</sub> uptake capacity of UTSA-280 was 3.0 mmol/g at 1 atm, 298 K and the density of CO<sub>2</sub> in the pore channel was up to 733 g/L, which was comparable to the liquid CO<sub>2</sub> density of ~1.1 kg/L (236 K, 11.1 bar), indicating that the CO<sub>2</sub> molecules in UTSA-280 were tightly packed. However, the relatively high isosteric heat of adsorption (Q<sub>st</sub>) of 42.9 kJ/mol was not favorable for material regeneration.

Another example of molecular sieving is Cu-F-pymo with dual functionality, exhibiting extremely high selectivity for CO<sub>2</sub> over CH<sub>4</sub> [52,56]. In Cu-F-pymo, Cu(II) atoms are coordinated to four N atoms from four different ligands to form a 1D pore channel with a pore diameter of ~3.3 Å. The IAST selectivity was calculated to be ultra-high, at 10<sup>7</sup> for CO<sub>2</sub>/CH<sub>4</sub> (v/v, 50/50) mixtures at 298 K and 1 bar. Grand canonical Monte Carlo (GCMC) simulation indicated that the binding affinity for CO<sub>2</sub> molecules was further enhanced by the pore channels functionalized with oxygen moieties through electrostatic and hydrogen bonding interactions. Furthermore, it could be easily synthesized in aqueous solution under ambient conditions. However, Cu-F-pymo showed a relatively low uptake capacity of 3.09 mmol/cm<sup>3</sup> (1.61 mmol/g) at 298 K and 1 bar due to the compact pore volume.

A higher CO<sub>2</sub> uptake achieved by molecular sieving adsorbent was achieved using SIFSIX-14-Cu-i [43]. SIFSIX-type MOFs are a typical kind of microporous MOF designed according to the isorecticular principle. These MOFs with 1D pores are composed of 2D metal–dipyridyl layers and SiF<sub>6</sub><sup>2−</sup>-type anion pillars in pcu topology. The replacement of organic ligands with different molecule lengths and/or framework interpenetrations provides extensive adjustment of the pore diameter, and the presence of F atoms in the channel tends to provide high affinity for CO<sub>2</sub> [57]. The pore cavity of SIFSIX-14-Cu-i was embellished with a high density of SiF<sub>6</sub><sup>2−</sup> anions and thus showed high CO<sub>2</sub> capacity (4.71 mmol/g) under ambient conditions.

Qc-5-Cu demonstrated a strategy of crystal engineering to tune pore size in MOFs (Figure 2) [42]. HQc (quinoline-5-carboxylic acid) and five kinds of metal ions were used to synthesize five different MOFs, Qc-5-M-dia (dia indicates a twofold and 3D diamondoid network) and Qc-5-Cu-sql- $\alpha$  (sql indicates a 2D square lattice network). Qc-5-Cu-sql- $\beta$  was the desolvated phase of Qc-5-Cu-sql- $\alpha$ , with a contract cell volume of  $1004.1 \pm 0.1$  to  $908.0 \pm 0.1$  Å<sup>3</sup> and a pore size of 3.8 to 3.3 Å. Such regulated channels of Qc-5-Cu-sql- $\beta$  fit the kinetic diameter of CO<sub>2</sub> and could exclude methane molecules, leading to high selectivity ( $\approx 3300$ ) for CO<sub>2</sub>. Qc-5-Cu-sql- $\beta$  also exhibited higher  $Q_{st}$  (36 kJ/mol) than its supramolecular isomer, Qc-5-Cu-dia (34 kJ/mol), and Qc-5-Ni-dia (32 kJ/mol). Molecular simulations of CO<sub>2</sub> adsorption revealed that the interaction sites were the H atoms in the Qc ligands, which could attract the negatively charged CO<sub>2</sub> oxygen atoms. In the modeled CO<sub>2</sub>-loaded structure, the distance between the O atoms and interaction sites was  $<2.5$  Å in Qc-5-Cu-sql- $\beta$  but  $>3.0$  Å in Qc-5-Ni-dia, which explains the difference in their adsorption behavior and  $Q_{st}$ . However, the CO<sub>2</sub> capacity of the former was only 2.16 mmol/g at 293 K, 1 bar, which is negative for practical applications.

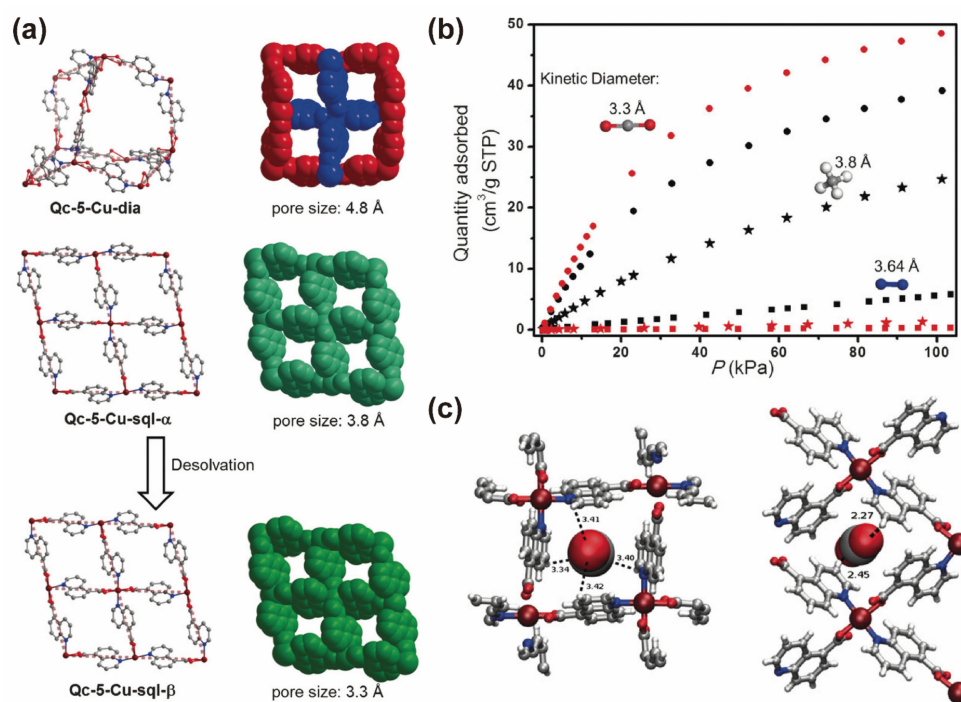


**Figure 2.** (a) Pore diameter tuning by supramolecular isomerism. (b) CO<sub>2</sub> (circle) and CH<sub>4</sub> (star) sorption isotherm for Qc-5-Cu-dia (black) and Qc-5-Cu-sql- $\beta$  (red) at 293 K. (c) The binding sites in the CO<sub>2</sub>-loaded Qc-5-Cu-dia (left) and Qc-5-Cu-sql- $\beta$  (right). Color code: C (gray), H (white), Cu (brown), N (blue), O (red). Reproduced with permission from Chen et al., *Angewandte Chemie International Edition*; published by John Wiley and Sons, 2016 [42].

Jiang et al. found a new strategy to precisely tune the multinuclear clusters of MOFs via symmetry-upgrading isoreticular transformation and obtained MOFs with high CO<sub>2</sub> selectivity [44]. As a precursor, Cu(IN)<sub>2</sub> (termed FZU, IN = isonicotinic acid) with binuclear clusters was used for isoreticular transformation towards NJU-Bai34 and NJU-Bai35 with clusters of higher symmetry (Figure 3). The binuclear cluster of FZU offered certain structural flexibility, and the uncoordinated O atoms made it possible to incorporate additional metal ions and upgrade the symmetry of the inorganic clusters without changing connectivity. With an increase in the concentration of Cu<sup>2+</sup> ions and the addition of water, acetonitrile and acetic acid, NJU-Bai34 was obtained from [Cu<sub>4</sub>(μ<sub>3</sub>-O)<sub>2</sub>(COO)<sub>4</sub>N<sub>4</sub>O<sub>2</sub>]. All Cu atoms in NJU-Bai34 were five-coordinated, and the remaining coordination sites were saturated by CH<sub>3</sub>COO<sup>-</sup>. However, the coordination of CH<sub>3</sub>COO<sup>-</sup> requires ((CH<sub>3</sub>)<sub>2</sub>NH<sub>2</sub>)<sup>+</sup> generated by DMF hydrolysis to neutralize the entire complex. Therefore, part of the pore channel is blocked by CH<sub>3</sub>COO<sup>-</sup> and the counterions. To avoid this phenomenon, the reaction was conducted at 120 °C using DMF/H<sub>2</sub>O as a solvent. The Cl atoms in copper chloride started to coordinate and shrunk the Cu clusters more than NJU-Bai34. After the symmetry of clusters was upgraded, the channels sizes of NJU-Bai35 were 3.6 × 3.6 Å<sup>2</sup> (along the *a* axis), 3.4 × 3.4 Å<sup>2</sup> (along the *b* axis) and 3.6 × 3.6 Å<sup>2</sup> (along the *c* axis) and perfectly fit the CO<sub>2</sub> molecules, which resulted in a higher CO<sub>2</sub> uptake capacity of 7.20 wt% than NJU-Bai34 and FZU at 298 K, 0.15 bar. Furthermore, NJU-Bai35 exhibited a high CO<sub>2</sub>/CH<sub>4</sub> selectivity of 11.6 for an equimolar mixture at 298 K, 1 bar, mainly due to the molecular sieve effect, with a pore size of 3.6 × 3.6 Å<sup>2</sup>. As a result, breakthrough curves further demonstrated that NJU-Bai35 has high potential for natural gas purification.

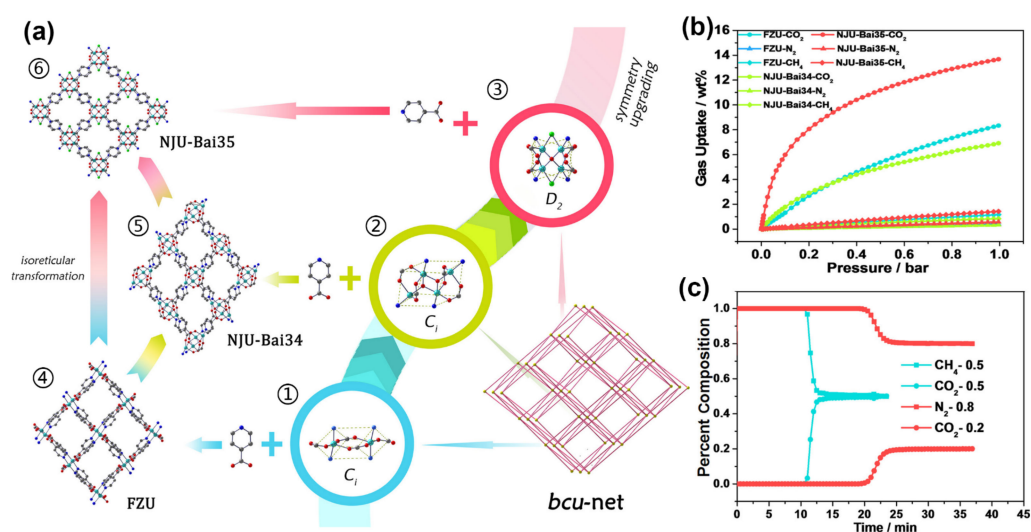


**Figure 3.** (a) Isoreticular transformation by symmetry-upgrading Cu clusters. Cu clusters and structures of FZU (1, 4), NJU-Bai34 (2, 5) and NJU-Bai35 (3, 6). (b) CO<sub>2</sub> adsorption isotherms measured at 298 K. (c) Breakthrough curves of NJU-Bai35 at 298 K. Reproduced with permission from Jiang et al., Journal of the American Chemical Society; published by American Chemical Society, 2018 [44].

Despite the extremely high selectivity, the strategy of molecular sieving typically suffers from low capacity limited by the compact pore volume, which is not favorable for MOF applications. The discrepancy in polarizability and acidity inspired some researchers to construct functional sites such as OMSs and Lewis basic sites with enhanced CO<sub>2</sub> interactions.

The open magnesium sites in Mg-MOF-74 were discovered by Bao et al. with high affinity for CO<sub>2</sub> [36]. At 298 K and 1 atm, the uptake of CO<sub>2</sub> was as high as 8.61 mol/kg (37.8 wt.%), which is significantly higher than that of the general amine-treated adsorbents. Comparatively, the uptake of CH<sub>4</sub> was only 1.05 mol/kg (1.7 wt.%), and the Henry's Law selectivity for CO<sub>2</sub>/CH<sub>4</sub> (50/50) was 8 at 298 K and 1 atm. Intense guest–framework interaction also induced an extremely high  $Q_{st}$  of 73 kJ/mol, which was not conducive to the regeneration of materials.

Amine functionalization is considered a feasible strategy to improve the CO<sub>2</sub> capture capacity of MOFs. PEI-incorporated amine-MIL-101(Cr) represented a polyethyleneimine-decorated MOF adsorbent [41]. After loading PEI, the structure of amine-MIL-101(Cr) was not degraded in scanning electron microscopy images; however, the pore size and polarity were affected as the PEI loading increased. Taking advantage of the porous characteristics of MIL-101(Cr) and Lewis basic –NH<sub>2</sub> groups, PEI-incorporated amine-MIL-101(Cr) showed a high CO<sub>2</sub> capacity of 3.6 mmol/g and an IAST selectivity of 931 for equimolar CO<sub>2</sub>/CH<sub>4</sub> mixtures under 100 kPa, 298 K.

In(aip)<sub>2</sub> is a 2D stacked MOF composed of In clusters and 5-aminoisophthalic acid with abundant amine groups (–NH<sub>2</sub>) in the channels, serving as hydrogen bonding sites and Bronsted basic sites to improve the interaction with CO<sub>2</sub> [48]. The Horvath–Kawazoe (HK) model determined the experimental average pore diameter of In(aip)<sub>2</sub> to be approximately 3.57 Å, which is between the molecular sizes of CH<sub>4</sub> and CO<sub>2</sub>. A synergetic size-sieving effect and –NH<sub>2</sub> interaction sites resulted in an extremely high IAST selectivity of 1808 for CO<sub>2</sub>/CH<sub>4</sub> (50/50, *v/v*) but limited uptake capacity of 1.27 mmol/g for CO<sub>2</sub> under ambient conditions.

Uncoordinated N donors as active sites could also enhance the CO<sub>2</sub> adsorption affinity and have been introduced into MOFs. Based on the MOF SYSU platform, two isorecticular MOFs, [Cu(L<sub>2</sub>)·DMF]<sub>∞</sub> (NJU-Bai7) and [Cu(L<sub>3</sub>)·DMF·H<sub>2</sub>O] (NJU-Bai8), were created by altering the coordination sites of the ligands and adjusting the pore size while introducing uncoordinated nitrogen atoms to the inner surface (Figure 4) [40]. The porosity and specific surface area of the three MOFs remained almost unchanged after channel narrowing and polarization. However, at low pressure (0.15 bar), NJU-Bai7 and NJU-Bai8 could adsorb 8.0 wt% and 5.4 wt% of CO<sub>2</sub> at 298 K, respectively—higher than the 3.6 wt% for SYSU. Both NJU-Bai7 and NJU-Bai8 showed much higher  $Q_{st}$  for CO<sub>2</sub> (40.5 and 37.7 kJ/mol, respectively) and separation ratios at 273 K (14.1 and 40.8, respectively) compared with the MOF SYSU platform, which may be attributed to the narrow channels, favoring the interaction with CO<sub>2</sub>. In contrast, NJU-Bai8 showed stronger CO<sub>2</sub> recognition and higher CO<sub>2</sub>/CH<sub>4</sub> selectivity than NJU-Bai7 because of unsaturated N atoms, which made it a better choice for trapping CO<sub>2</sub> from the CO<sub>2</sub>/CH<sub>4</sub> mixture.

IRHs-(1–3) are three isorecticular lanthanide MOFs from cyamelurate linkers characterized by a large number of accessible N-donor sites [47]. Due to the abundant uncoordinated N on the hydrophilic pore walls, the interaction with CO<sub>2</sub> was enhanced, and CH<sub>4</sub> with non-polar covalent bonds was excluded, facilitating the adsorption of CO<sub>2</sub> over CH<sub>4</sub>. Through GCMC simulations, researchers found that no CH<sub>4</sub> was distributed around the metal center as a result of the existence of water molecules. The uptake of CO<sub>2</sub> and CH<sub>4</sub> in IRH-3 was 2.7 and 0.07 mmol/g, respectively, and the IAST selectivity for equimolar CO<sub>2</sub>/CH<sub>4</sub> reached 27 at 298 K and 1 bar.

3-amino-1,2,4-triazole (Hatz) was used to produce a zeolite-like MOF, [Zn(atz)<sub>2</sub>] (MAF-66), at room temperature with –NH<sub>2</sub> groups and uncoordinated triazolone nitrogen atoms in the channels [37]. MAF-66 exhibited a high CO<sub>2</sub> uptake capacity of 4.41 mol/kg, and the IAST selectivity for equimolar CO<sub>2</sub>/CH<sub>4</sub> was 5.8 at 298 K and 1 bar. The  $Q_{st}$  of MAF-66 at zero coverage was 26.0 kJ/mol, which is significantly lower than those of PCPs based on OMSs. A low  $Q_{st}$  is beneficial to the adsorption–desorption cycle of the material.

UiO-66(N<sub>10%</sub>-Zr) was designed through the in situ functionalization of node chemistry of UiO-66 with 2-aminobenzimidazole (2-AMI) by a novel microwave-assisted strategy [50]. The grafted 2-AMI on the nodes provided the N-containing five-membered heterocycle as an electron donor. Through electrostatic interactions, -NH<sub>2</sub> could act as a binding site for Lewis acidic CO<sub>2</sub> and produce a specific recognition effect. The stability and hydrophobicity would also be enhanced because the benzene ring in 2-AMI modified the frameworks, making them inert. The node-engineered UiO-66(N<sub>10%</sub>-Zr) showed excellent separation performance for CO<sub>2</sub>/CH<sub>4</sub> through a synergetic equilibrium–kinetic effect. The CO<sub>2</sub> uptake was 2.1 mol/kg, and the IAST selectivity was up to 326 for a 50/50 CO<sub>2</sub>/CH<sub>4</sub> mixture at 298 K, 1 atm—both higher than those of UiO-66. The  $Q_{st}$  of UiO-66(N<sub>10%</sub>-Zr) was 35.7 kJ/mol, which is also higher than the  $Q_{st}$  of UiO-66 (22.0 kJ/mol), indicating that node-engineering contributed to the stronger affinity for CO<sub>2</sub>.

The low-cost and water-stable SIFSIX-1-Cu [Cu(bpy)<sub>2</sub>(SiF<sub>6</sub>)] exhibited an extremely high capacity of 5.2 mmol/g for CO<sub>2</sub> at 298 K, 1 atm, and a high selectivity of 10.5 for an equimolar CO<sub>2</sub>/CH<sub>4</sub> mixture [38]. Furthermore, the  $Q_{st}$  value for CO<sub>2</sub> was as low as 27 kJ/mol. SIFSIX-2-Cu and SIFSIX-2-Cu-i were both synthesized from the reaction of 4,4'-dipyridylacetylene (dpa) and CuSiF<sub>6</sub>. SIFSIX-2-Cu-i was isostructural to SIFSIX-2-Cu but with double interpenetrated nets [39]. After interpenetrating, the pore size formed by SIFSIX-2-Cu-i was smaller than that of SIFSIX-2-Cu (13.05 Å), which was 5.15 Å. Similarly, SIFSIX-3-Zn was synthesized from the shorter pyrazine and thus resulted in smaller pore size of 3.84 Å (Figure 5). Owing to its optimal pore size, the electropositive carbon atoms of CO<sub>2</sub> molecules could closely interact with the fluorine atoms of SiF<sub>6</sub><sup>2-</sup> and provided a benchmark IAST selectivity of 231 for a 50/50 CO<sub>2</sub>/CH<sub>4</sub> mixture. This research demonstrates the successful control of pore size according to the isorecticular principle. Together with the favorable electrostatic interactions provided by the inorganic anion array, the SIFSIX series MOFs are capable of a synergetic equilibrium–kinetic effect, allowing for the separation of CO<sub>2</sub> mixtures, with the potential for high selectivity, recoverability and moisture stability.

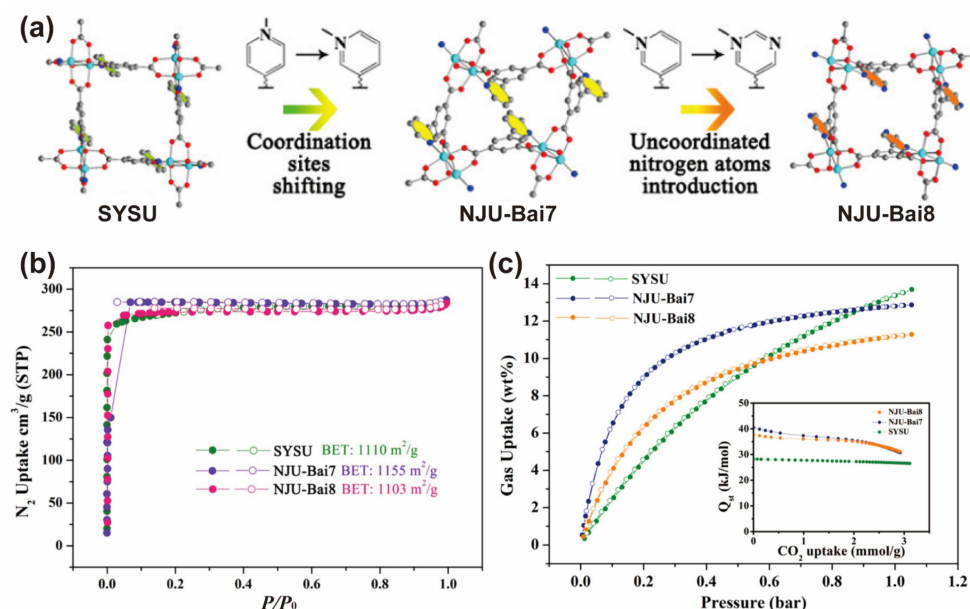


**Figure 4.** (a) Structure of SYSU (left), NJU-Bai7 (middle) and NJU-Bai8 (right). (b) N<sub>2</sub> sorption isotherms for SYSU, NJU-Bai7 and NJU-Bai8 at 77 K. (c) CO<sub>2</sub> sorption isotherms and CO<sub>2</sub> adsorption enthalpy (insert) for SYSU, NJU-Bai7 and NJU-Bai8 at 298 K. Reproduced with permission from Du et al., Journal of the American Chemical Society; published by American Chemical Society, 2013 [40].

For the mixture system of  $\text{CO}_2$  and  $\text{CH}_4$ ,  $\text{CO}_2$  has a smaller molecular size and is more acidic and can therefore be easily separated by the strategy of molecular sieving and construction of strong  $\text{CO}_2$  binding sites. It should be noted that although ultra-high selectivity can be achieved using a molecular sieving mechanism, the narrowed pore channels often tend to result in low adsorption capacity. Therefore, future studies should investigate the construction of pore structures with large cavities connected by narrow pore channels, potentially maintaining a large adsorption capacity while sieving at a narrow entrance with high selectivity.

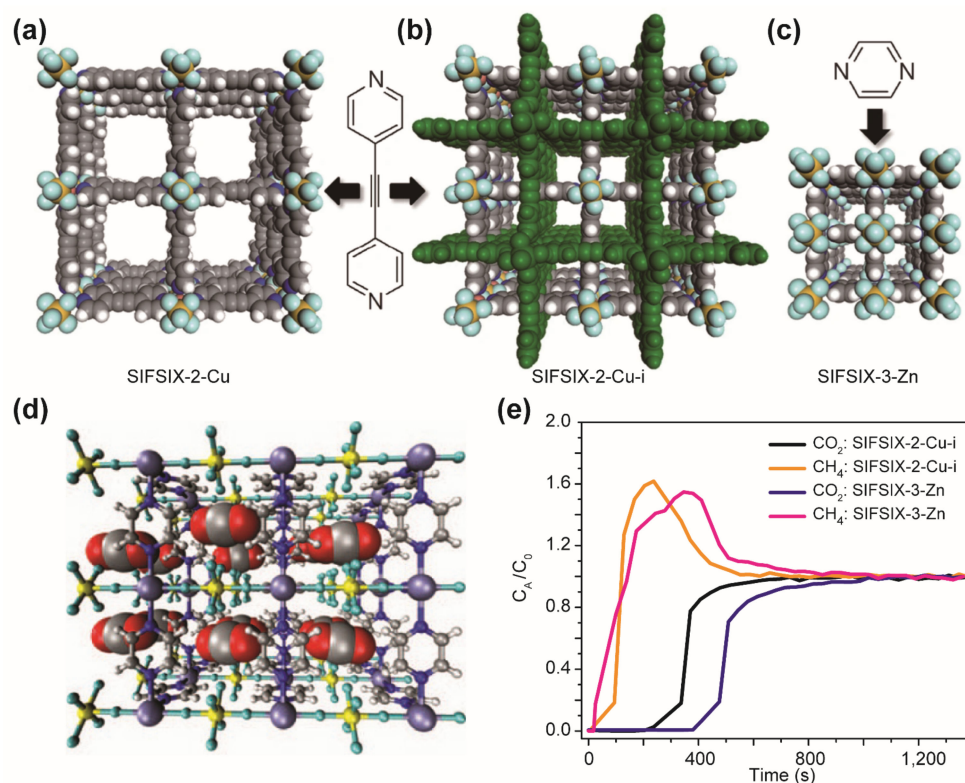


**Figure 5.** (a–c) Schematic diagram of the frameworks of SIFSIX-2-Cu (a), SIFSIX-2-Cu-i (b) and SIFSIX-3-Zn (c). Color code: Si (yellow), C (gray), F (light blue), N (blue), H (white). For clarity, the green structure indicates the interpenetrated network. (d) Structure diagram of interactions between the  $\text{CO}_2$  molecules and  $\text{SiF}_6^{2-}$ . Color code: C (gray), F (green), N (blue), Si (yellow), O (red), H (white), Zn (purple). (e) Breakthrough curves for a  $\text{CO}_2/\text{CH}_4$  (50/50) mixture for SIFSIX-2-Cu-i and SIFSIX-3-Zn at 298 K, 1 atm. Reproduced with permission from Nugent et al., Nature; published by Springer Nature, 2013 [39].

### 3. $\text{CO}_2$ -Selective Capture from $\text{CO}_2/\text{C}_2\text{H}_2$ Mixture

$\text{C}_2\text{H}_2$  is an important fuel for the welding industry and an essential feedstock used to fabricate petrochemical products. Among the gas mixtures of acetylene, the separation of  $\text{C}_2\text{H}_2/\text{CO}_2$  is the most important and challenging due to the ultra-high similarity of these compounds in molecular size, shape and boiling points (Table 1). Moreover, most of reported MOF materials interact more strongly with  $\text{C}_2\text{H}_2$  than  $\text{CO}_2$ , as the hydrogens and  $\pi$ -electrons on  $\text{C}_2\text{H}_2$  are highly polarizable and acidic and usually interact with acid–base interaction sites. Such  $\text{C}_2\text{H}_2$  selectivity is called “normal selectivity” and suffers from two energy-intensive steps of adsorption and desorption to obtain pure  $\text{C}_2\text{H}_2$  gas [58–66].  $\text{CO}_2$  capture from  $\text{C}_2\text{H}_2/\text{CO}_2$  in one step is more energy-efficient for purification of  $\text{C}_2\text{H}_2$ , saving approximately 40% energy by eliminating other complex post-regeneration operations [22]. Therefore, ideal physisorbents should preferentially capture the trace  $\text{CO}_2$  from the gas mixture rather than  $\text{C}_2\text{H}_2$  (“inverse selectivity”) to further reduce the energy consumption of  $\text{C}_2\text{H}_2/\text{CO}_2$  separation [25,67,68].

In the past few years, various benchmark MOFs have been demonstrated to exhibit “inverse selectivity” for CO<sub>2</sub>/C<sub>2</sub>H<sub>2</sub> separation, as shown in Table 3. Owing to their very close kinetic diameters, it is difficult to separate CO<sub>2</sub>/C<sub>2</sub>H<sub>2</sub> with the molecular sieve mechanism. Generally, the following strategies are utilized: (1) exploiting the structural flexibility or phase transition induced by different gas molecules, (2) optimizing pore chemistry through different electrostatic interactions or thermodynamic affinity and (3) constructing kinetic diffusivity differences through precise pore geometry.

**Table 3.** Representative MOFs for CO<sub>2</sub>-selective capture from CO<sub>2</sub>/C<sub>2</sub>H<sub>2</sub> mixture \*.

MOF	Functional Site	CO <sub>2</sub> Capacity (mmol/g)	CO <sub>2</sub> /C <sub>2</sub> H <sub>2</sub> Selectivity	Q <sub>st</sub> for CO <sub>2</sub> (kJ/mol)	Ref.
Co(HL <sup>dc</sup> )	gate opening	10.69 <sup>a</sup>	1.7 <sup>a,b</sup>	—	[69]
[Mn(bdc)(dpe)]	gate opening	2.17 <sup>c</sup>	8.8 <sup>c</sup>	29.5	[70]
SIFSIX-3-Ni	SiF <sub>6</sub> <sup>2-</sup>	2.7	7.69 <sup>d</sup>	50.9	[71]
CD-MOF-1	uncoordinated primary hydroxyl groups	2.87	6.6 <sup>d</sup>	41.0	[72]
CD-MOF-2	uncoordinated primary hydroxyl groups	2.65	16 <sup>d</sup>	67.2	[72]
[Tm <sub>2</sub> (OH-bdc)] (1a)	OH groups	5.83	17.5 <sup>d</sup>	45.2	[73]
[Tm <sub>2</sub> (OH-bdc)] (1a')	OH groups	6.21	1.65 <sup>d</sup>	32.7	[73]
PCP-NH <sub>2</sub> -bdc	amino group	3.03	4.4	34.57	[74]
PCP-NH <sub>2</sub> -ipa	amino group	3.21	6.4	36.6	[74]
Cd-NP	electrostatic potential	2.59	85	27.7	[75]
Ce <sup>IV</sup> -MIL-140-4F	electrostatic potential	2.24	9.5	39.5	[76]
Cu-F-pymo	electrostatic potential	1.19	10 <sup>5</sup>	28.8	[77]
[Zn(atz)(BDC-Cl <sub>4</sub> ) <sub>0.5</sub> ln]	electrostatic potential	0.94 <sup>f,g</sup>	2.4 <sup>f</sup>	32.7	[78]
PMOF-1(irra)	electrostatic potential	2.38 <sup>c</sup>	694 <sup>c</sup>	—	[79]
MUF-16	electrostatic potential	2.13 <sup>e</sup>	510 <sup>e</sup>	32.3	[51]
MUF-16(Mn)	electrostatic potential	2.25 <sup>e</sup>	31 <sup>e</sup>	36.6	[51]
MUF-16(Ni)	electrostatic potential	2.13 <sup>e</sup>	46 <sup>e</sup>	37.3	[51]
en-MOF	amine groups	4.8	—	71.2	[80]
nmen-MOF	amine groups	4.55	—	62.3	[80]
een-MOF	amine groups	4.9	—	68.8	[80]
ZU-610a	kinetic sieving	1.51	207	27.3	[81]
SU-101(Bi)	carbonyl oxygen atoms	2.4	5.5	30.5	[82]
SU-101(Al)	carbonyl oxygen atoms	2.37	15.5	31.3	[82]
SU-101(In)	carbonyl oxygen atoms	2.46	6.2	28.3	[82]
SU-101(Ga)	carbonyl oxygen atoms	1.79	11.1	27.7	[82]
[Zn(odip) <sub>0.5</sub> (bpe) <sub>0.5</sub> ]	Gate Opening	5.3	13.2	42.3	[54]

\* Unless otherwise specified, the capacity data were all recorded at 1 bar, 298 K; CO<sub>2</sub>/C<sub>2</sub>H<sub>2</sub> selectivity is IAST selectivity for 50/50 (v/v) CO<sub>2</sub>/C<sub>2</sub>H<sub>2</sub> mixtures at 1 bar, 298 K; Q<sub>st</sub> for CO<sub>2</sub> is the value at zero coverage; “—” indicates that data were not found; <sup>a</sup> at 195 K; <sup>b</sup> calculated by uptake ratio; <sup>c</sup> at 273 K; <sup>d</sup> selectivity for CO<sub>2</sub>/C<sub>2</sub>H<sub>2</sub> (1/2, v/v); <sup>e</sup> at 293 K; <sup>f</sup> at 285 K; <sup>g</sup> calculated by (volumetric uptake)/(crystal density).

It has been reported that some flexible MOFs can achieve efficient separation of highly challenging gas mixtures by mechanisms such as guest-induced “gate opening”. The structural flexibility and/or phase transition of flexible MOFs leads to an abrupt increment in uptake amount at a critical pressure, i.e., a “step” adsorption isotherm [83–87].

[Co(HL<sup>dc</sup>)] is a dynamic bifunctional MOF with inverse CO<sub>2</sub>/C<sub>2</sub>H<sub>2</sub> selectivity [69]. The framework flexibility of [Co(HL<sup>dc</sup>)] is provided by the dangling carboxylic groups and electron-donating nitrogen centers on the channel surface, showing gated adsorption for CO<sub>2</sub> instead of C<sub>2</sub>H<sub>2</sub>. At 195 K, symmetric CO<sub>2</sub> molecules with a permanent quadrupole moment can interact with the MOF frameworks and lead to the rotation of pyridyl rings, opening the “gate”. However, C<sub>2</sub>H<sub>2</sub> could not trigger a similar “gate” rotation because the adsorption temperature (195 K) was higher than its boiling point (189 K), and therefore, more C<sub>2</sub>H<sub>2</sub> uptake was required. The CO<sub>2</sub> uptake capacity was 10.69 mol/kg at 195 K, 1 bar, and the CO<sub>2</sub>/C<sub>2</sub>H<sub>2</sub> uptake ratio was 1.7.

Another flexible MOF with inverse  $\text{CO}_2/\text{C}_2\text{H}_2$  selectivity is  $[\text{Mn}(\text{bdc})(\text{dpe})]$  [70]. Its small zero-dimensional pores showed gated adsorption for  $\text{C}_2\text{H}_2$  instead of  $\text{CO}_2$  due to their opposite quadrupole moments, resulting in different  $\text{CH}-\pi$  and  $\pi-\pi$  interactions. The adsorption isotherm of  $\text{C}_2\text{H}_2$  showed a gated behavior at a gate-opening pressure ( $P_{\text{go}}$ ) of 1.45 kPa at 195 K, whereas  $\text{CO}_2$  did not. The  $\text{CO}_2$  uptake amount was 2.17 mmol/g at 273 K, 100 kPa, and the IAST selectivity for  $\text{CO}_2/\text{C}_2\text{H}_2$  ( $v/v$ , 50/50) gas mixture varied from 8.8 to 13, indicating the excellent potential for  $\text{CO}_2$  capture from a  $\text{CO}_2/\text{C}_2\text{H}_2$  mixture. In situ X-ray diffraction (XRD) and density functional theory (DFT) calculations illustrate that due to the opposite quadrupole moment, the electrostatic potential of the pore leads to repulsion with  $\text{C}_2\text{H}_2$  in an end-on orientation, requiring more structural transformation energy to adapt to  $\text{C}_2\text{H}_2$  with a side-on orientation (Figure 6).

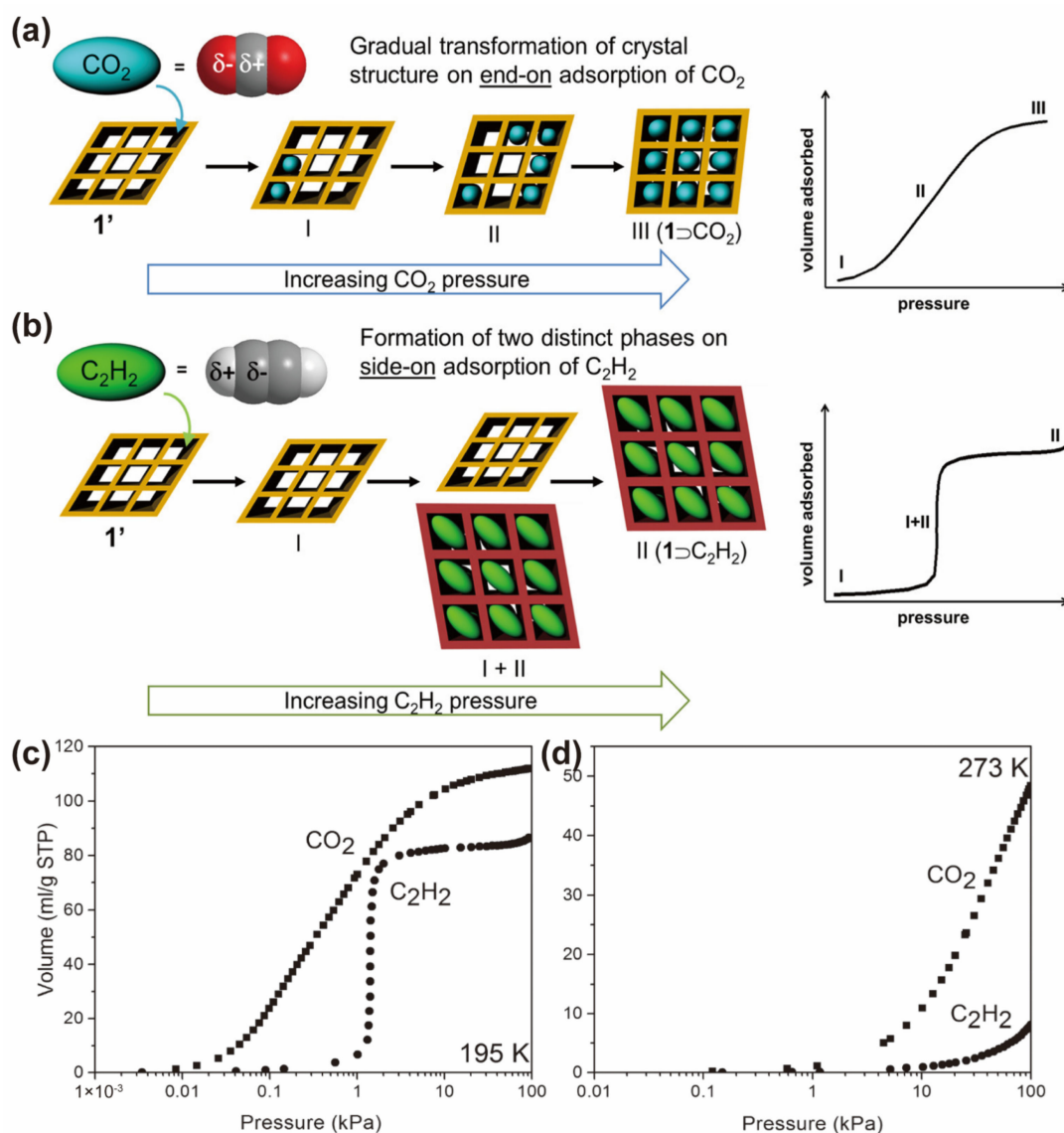


**Figure 6.** (a,b) Potential adsorption mechanism of  $[\text{Mn}(\text{bdc})(\text{dpe})]$  for  $\text{CO}_2$  (a) and  $\text{C}_2\text{H}_2$  (b) at 195 K. (c,d) Adsorption isotherms of  $[\text{Mn}(\text{bdc})(\text{dpe})]$  for  $\text{CO}_2$  and  $\text{C}_2\text{H}_2$  at 195 K (c) and 273 K (d). Reproduced with permission from Foo et al., Journal of the American Chemical Society; published by American Chemical Society, 2016 [70].

The opposite quadrupole moments of CO<sub>2</sub> ( $-13.4 \times 10^{-40} \text{ C m}^2$ ) and C<sub>2</sub>H<sub>2</sub> ( $+20.5 \times 10^{-40} \text{ C m}^2$ ) have enlightened researchers to adjust the pore environment with inverse electrostatic potential (ESP) or precise steric arrangement of interaction sites on the pore surface, which is more favorable for CO<sub>2</sub> adsorption and leads to inverse CO<sub>2</sub>/C<sub>2</sub>H<sub>2</sub> separation [74].

Cd[Fe(CN)<sub>5</sub>NO] (Cd-NP) is an ultra-microporous MOF constructed by 3.2 Å pore channels connecting ellipsoidal cavities, which are analogous to the molecular shapes of CO<sub>2</sub> and C<sub>2</sub>H<sub>2</sub> [75]. The ESP of the pore surface mapped by DFT calculations shows a positive potential ( $\alpha$ ) around the Cd center, a positive potential ( $\beta$ ) on the N atom of nitrosyl and a negative potential ( $\gamma$ ) near the N atom of cyanide. Therefore, the ESP of the pore surface was complementary to CO<sub>2</sub> rather than C<sub>2</sub>H<sub>2</sub>. Cd-NP provided a high CO<sub>2</sub> capacity of 2.59 mol/kg and an IAST selectivity of 85 for an equimolar CO<sub>2</sub>/C<sub>2</sub>H<sub>2</sub> gas mixture at 298 K, 1 atm. The calculated  $Q_{\text{st}}$  for CO<sub>2</sub> at near-zero coverage was 27.7 kJ/mol, which supported the viability of regeneration under mild conditions.

Zhang et al. proposed that metal nodes in a highly oxidized state can attract electrons from the ligands, generating a pore surface with more polarities that preferentially recognize CO<sub>2</sub> molecules [76]. Therefore, they synthesized Ce<sup>IV</sup>-MIL-140-4F from tetrafluoro terephthalate and Ce<sup>IV</sup> with unoccupied 4f orbitals. Ce<sup>IV</sup>-MIL-140-4F provided an optimal pore environment to specifically trap CO<sub>2</sub> via strong host-guest interactions, whereas the isostructural Zr<sup>IV</sup>-MIL-140-4F exhibited normal C<sub>2</sub>H<sub>2</sub> selectivity over CO<sub>2</sub>. The ESP distributions illustrate that there are two different electron regions at the edge of the channel of the two MIL-140-4F MOFs (electron-rich region I and electron-poor region II). (Figure 7). Compared with Zr<sup>IV</sup>-MIL-140-4F, the electron cloud density of Ce<sup>IV</sup>-MIL-140-4F was higher at site I, and the potential was more positive at site II. In situ PXRD and in situ FTIR spectra indicate that CO<sub>2</sub> was perfectly located on site I of Ce<sup>IV</sup>-MIL-140-4F and bound by four fluorine atoms with strong F...C=O interactions. In contrast, DFT calculations indicate that C<sub>2</sub>H<sub>2</sub> was located on site II of Ce<sup>IV</sup>-MIL-140-4F with weaker  $\equiv\text{C}-\text{H}\cdots\text{F}$  interactions. The different binding configurations of CO<sub>2</sub> and C<sub>2</sub>H<sub>2</sub> in Ce<sup>IV</sup>-MIL-14-4F resulted in a superior CO<sub>2</sub> capacity of 110.3 cm<sup>3</sup>/cm<sup>3</sup> (2.24 mmol/g) and an excellent separation selectivity of  $\sim 9.5$  for 50/50 CO<sub>2</sub>/C<sub>2</sub>H<sub>2</sub> mixtures at 298 K, 100 kPa. Furthermore, the  $Q_{\text{st}}$  for CO<sub>2</sub> and C<sub>2</sub>H<sub>2</sub> on Ce<sup>IV</sup>-MIL-140-4F was 39.5 and 27.4 kJ/mol, respectively, showing stronger affinity to CO<sub>2</sub> than C<sub>2</sub>H<sub>2</sub>.

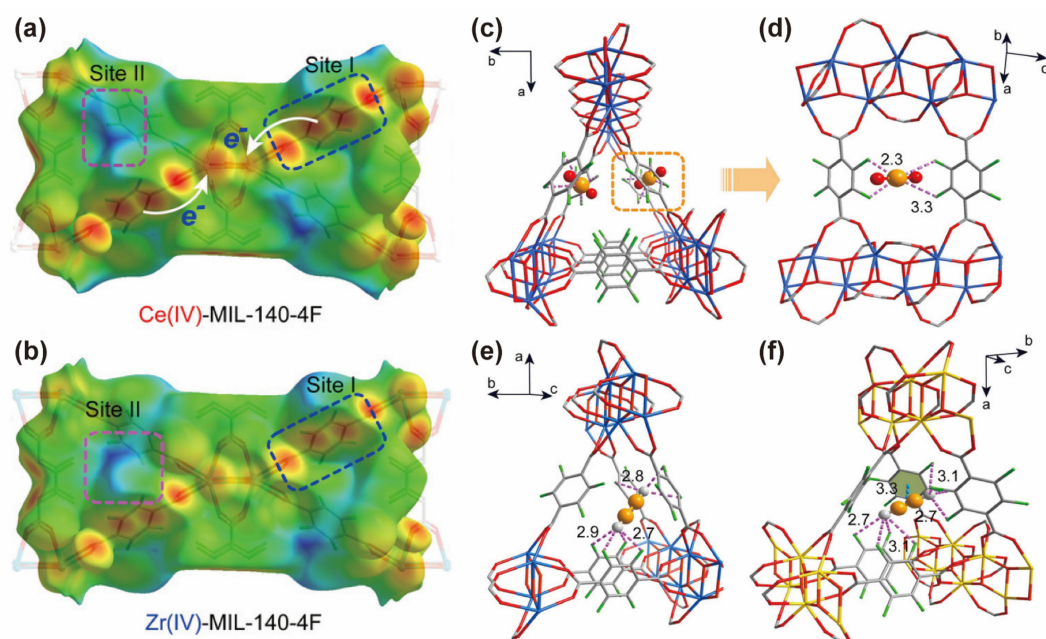


**Figure 7.** (a,b) The Hirshfeld surface with  $d_e$  (ESP) in  $\text{Ce}^{\text{IV}}\text{-MIL-140-4F}$  (a) and  $\text{Zr}^{\text{IV}}\text{-MIL-140-4F}$  (b) (gradient color from red to blue indicates changes in electron density from high to low). (c,d) Structure of  $\text{CO}_2$ -loaded  $\text{Ce}^{\text{IV}}\text{-MIL-140-4F}$  and the interaction between  $\text{CO}_2$  and F atoms. (e,f) The binding sites of  $\text{C}_2\text{H}_2$  in  $\text{Ce}^{\text{IV}}\text{-MIL-140-4F}$  (e) and  $\text{Zr}^{\text{IV}}\text{-MIL-140-4F}$  (f). Reproduced with permission from Zhang et al., *Angewandte Chemie International Edition*; published by John Wiley and Sons, 2021 [76].

$\text{Cu-F-pymo}$  was constructed by Shi et al. from 5-fluoropyrimidin-2-olate for inverse  $\text{CO}_2$  selectivity [77]. They found that residual solvent molecules under different conditions could provide sites for gas molecules to realize high separation performance. GCMC simulation and DFT were used to calculate ESP, revealing that  $\text{CO}_2$  and  $\text{C}_2\text{H}_2$  molecules were preferentially adsorbed in different pores but the  $\text{C}_2\text{H}_2$ -preferential pore A was occupied by residual water molecules.  $\text{CO}_2$  could still be collected with three molecules per unit cell. At 1 atm, 298 K, the partly dehydrated  $\text{Cu-F-pymo}$  exhibited a  $\text{CO}_2$  adsorption capacity of 1.19 mmol/g and benchmark  $\text{CO}_2/\text{C}_2\text{H}_2$  selectivity of over  $10^5$  for the equimolar  $\text{CO}_2/\text{C}_2\text{H}_2$  mixture.

$[\text{Zn}(\text{atz})(\text{BDC-Cl4})_{0.5}]_n$  is a 3D pillared-layer ultra-microporous MOF constructed with electronegative Cl atoms embedded in the pore surface for inverse  $\text{CO}_2/\text{C}_2\text{H}_2$  separation [78].  $[\text{Zn}(\text{atz})(\text{BDC-Cl4})_{0.5}]_n$  showed an adsorption selectivity of 2.4 for a  $\text{CO}_2/\text{C}_2\text{H}_2$  (50/50) mixture at 285 K and 100 kPa and a  $Q_{\text{st}}$  of 32.7 kJ/mol for  $\text{CO}_2$ . The  $\text{CO}_2$ -selectivity resulted from a match between the pore surface adorned with Cl atoms and the quadrupole moment of  $\text{CO}_2$ . However,  $[\text{Zn}(\text{atz})(\text{BDC-Cl4})_{0.5}]_n$  could only adsorb  $\text{CO}_2$  with a capacity of  $34.6 \text{ cm}^3/\text{cm}^3$  (0.94 mol/kg) at 285 K, 1 bar.

Cai et al. proposed a photoinduced electron-transfer (PIET) strategy to modulate the electrostatic gradient of MOFs for selective adsorption of  $\text{CO}_2$  over  $\text{C}_2\text{H}_2$  [79]. Researchers found that the intrinsic electric field gradients of zwitterions were favorable for selective  $\text{CO}_2$  adsorption and that the radical  $\pi$  moieties generated by photoelectron transfer had strong affinity for the  $\pi$  systems of  $\text{CO}_2$ . During the PIET process, electrons were transferred from the oxygen-containing carboxylic acid ligand to the zwitterion, which would not change the electric field gradient of the material and prevent a decrease in  $\text{CO}_2$  adsorption. However, after the loss of one electron, the O atom could not form  $\text{H-C}\equiv\text{C-H}\cdots\text{O}$  hydrogen bonds with  $\text{C}_2\text{H}_2$  easily, reducing the adsorption of  $\text{C}_2\text{H}_2$  (Figure 8). Based on this strategy, the authors synthesized PMOF-1, which achieved a  $\text{CO}_2$  uptake of  $47.5 \text{ cm}^3/\text{g}$  before irradiation and  $53.3 \text{ cm}^3/\text{g}$  after irradiation for 1 h at 273 K and 100 kPa. The uptake ratio was also enhanced from 5.0 to 7.1. Notably, the IAST selectivity for an equimolar

$\text{CO}_2/\text{C}_2\text{H}_2$  mixture reached 694 at 273 K, 1 bar, which was superior to any other porous material reported for inverse  $\text{CO}_2$  adsorption over  $\text{C}_2\text{H}_2$ .

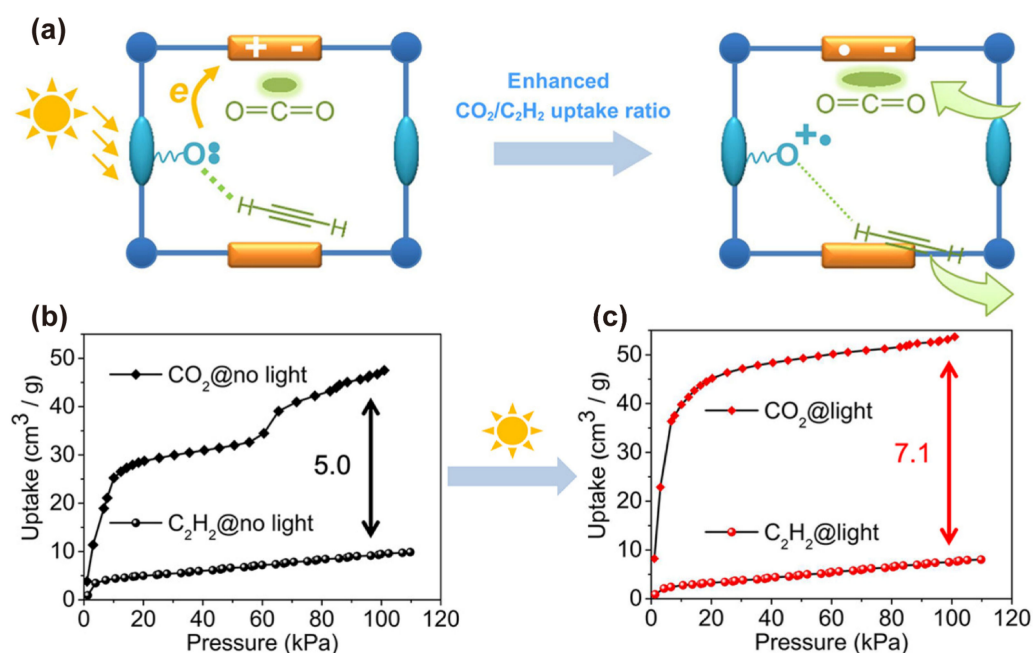


**Figure 8.** (a) PIET strategy for improving the uptake ratio of  $\text{CO}_2/\text{C}_2\text{H}_2$ . (b,c) Adsorption isotherms of  $\text{C}_2\text{H}_2$  and  $\text{CO}_2$  before (b) and after (c) irradiation at 273 K. Reproduced with permission from Cai et al., *Angewandte Chemie International Edition*; published by John Wiley and Sons, 2021 [79].

Pore chemistry can also be optimized through a precise steric arrangement of interaction sites for favorable  $\text{CO}_2$  adsorption on the pore surface. Gu et al. demonstrated the strategy of “opposite action” in MOFs, realizing the  $\text{CO}_2$  selective adsorption and separation of  $\text{CO}_2/\text{C}_2\text{H}_2$  under ambient temperature and pressure [74]. They synthesized two isostructural MOFs, PCP-NH<sub>2</sub>-bdc and PCP-NH<sub>2</sub>-ipa, from meso- $\alpha,\beta$ -di(4-pyridyl) glycol (dpg), terephthalic acid (bdc) and isophthalic acid (ipa). Owing to the different electronic structures of  $\text{CO}_2$  and  $\text{C}_2\text{H}_2$ , they tended to exhibit different binding orientations when adsorbed in microporous channels. Therefore, the precise encoding of interaction sites (-NH<sub>2</sub>) parallel to the  $\text{CO}_2$  binding site in the channel could enhance the  $\text{CO}_2$ -framework interaction without significantly changing the adsorption orientation of the  $\text{CO}_2$  molecules. On the contrary, the additional interaction sites could impact the adsorption orientation of  $\text{C}_2\text{H}_2$  and combine with the spatial restriction of the 1D confined channel to inhibit  $\text{C}_2\text{H}_2$  adsorption at other sites, ultimately achieving high  $\text{CO}_2/\text{C}_2\text{H}_2$  selectivity of more than 4.4 (Figure 9). PCP-NH<sub>2</sub>-bdc and PCP-NH<sub>2</sub>-ipa exhibited remarkably high  $\text{CO}_2$  uptake of 3.03 and 3.21 mmol/g, respectively. The  $Q_{\text{st}}$  at zero coverage of  $\text{CO}_2$  for PCP-NH<sub>2</sub>-bdc and PCP-NH<sub>2</sub>-ipa was reduced to 34.57 and 36.6 kJ/mol, respectively, indicating reduced energy consumption for regeneration and recycling.

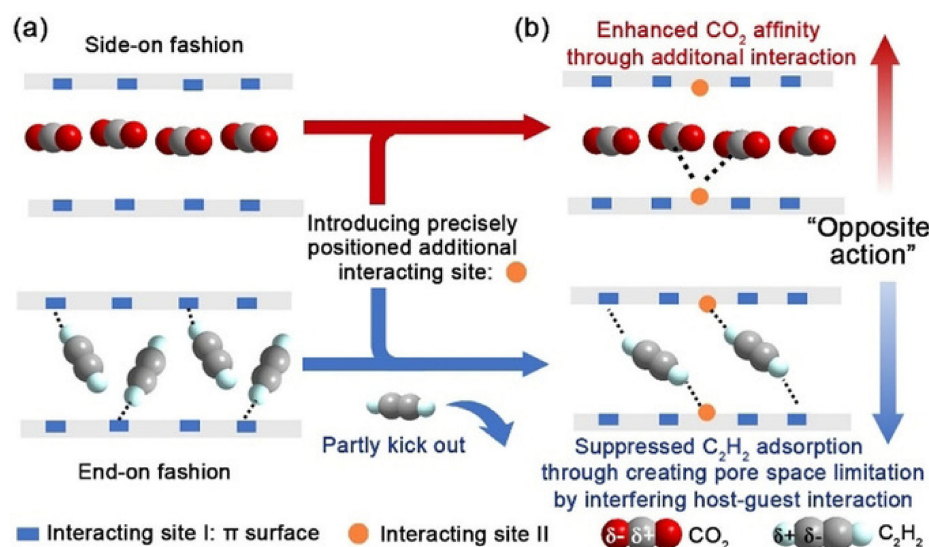


**Figure 9.** Schematic diagram of the “opposite action” strategy to improve CO<sub>2</sub> selectivity. (a) Different orientations of CO<sub>2</sub> and C<sub>2</sub>H<sub>2</sub> into the channel. (b) Precise steric arrangement of interaction sites providing an enhanced CO<sub>2</sub>–framework interactions and inhibiting C<sub>2</sub>H<sub>2</sub> adsorption. Reproduced with permission from Gu et al., *Angewandte Chemie International Edition*; published by John Wiley and Sons, 2021 [74].

SIFSIX-type MOFs were reported to provide high affinity for CO<sub>2</sub> via extensive adjustable pore size and electron-rich F atoms on the channel surface [57]. For instance, in SIFSIX-3-Ni, each CO<sub>2</sub> molecule was located near four F atoms of four SiF<sub>6</sub><sup>2-</sup> anions with a short distance of ~2.75 Å between C and F [71]. SIFSIX-3-Ni exhibited a high CO<sub>2</sub>/C<sub>2</sub>H<sub>2</sub> capacity of 2.5/2.0 mmol/g at 298 K, 0.1 bar, and a selectivity of 7.69 for CO<sub>2</sub>/C<sub>2</sub>H<sub>2</sub> (2/1; *v/v*) at 298 K, 1.0 bar. However, with a comparable pore environment, the analogous TIFSIX-2-Cu-i could only provide normal C<sub>2</sub>H<sub>2</sub> selectivity over CO<sub>2</sub>. The inverse “yin-yang” behavior in two analogous MOFs was explained by the different geometry of host–guest binding sites.

Thulium(iii)-based MOFs embellished with -OH groups and H<sub>2</sub>O [Tm<sub>2</sub>(OH-bdc)] with partly and fully dehydrated phases were termed **1a** and **1a'**, respectively [73]. With its optimized pore size and pore surface modified with -OH groups that could interact reversibly with CO<sub>2</sub> through hydrogen bonding, **1a** showed a high CO<sub>2</sub> capacity of 5.83 mol/kg and an IAST selectivity of 17.5 for CO<sub>2</sub>/C<sub>2</sub>H<sub>2</sub> (1/2, *v/v*) at 100 kPa, 298 K. The  $Q_{st}$  of CO<sub>2</sub> on **1a** was 45.2 kJ/mol, which is significantly higher than the  $Q_{st}$  of C<sub>2</sub>H<sub>2</sub> (17.8 kJ/mol), showing its strong affinity for CO<sub>2</sub>. The completely dehydrated phase **1a'** with both hydroxyl groups and open metal sites also provided a CO<sub>2</sub> capacity of 6.21 mmol/g but lower selectivity of only 1.65 under the same conditions.

Recently, a new kinetic sieving strategy for C<sub>2</sub>H<sub>2</sub>/CO<sub>2</sub> separation was demonstrated by ZU-610a with sulfonic anion pillars [81]. ZU-610a was obtained by heat treatment of ZU-610. The pore size was reduced from 3.8 Å and 4.7 Å to 3.2 Å and 4.1 Å after heat treatment, but the topology remained unchanged. Interestingly, after shrinking the pore size, the C<sub>2</sub>H<sub>2</sub>-selectivity of ZU-610 was reversed to the CO<sub>2</sub> selectivity of ZU-610a, due to the separation process, which transformed thermodynamic control into kinetic control. Kinetic adsorption studies revealed that CO<sub>2</sub> achieved equilibrium after ~10 min on Zu-610 and Zu-610a. However, C<sub>2</sub>H<sub>2</sub> did not reach equilibrium until 70 min (Figure 10). The absorption of CO<sub>2</sub> on Zu-610a was reduced slightly (1.51 mmol/g) due to pore shrinking, but the capacity of C<sub>2</sub>H<sub>2</sub> fell drastically from 3.22 to 0.12 mmol/g at 100 kPa, 298 K. Profiting from kinetic sieving, ZU-610a showed a selectivity of up to 207 for an equimolar CO<sub>2</sub>/C<sub>2</sub>H<sub>2</sub> mixture, which is higher than that of many benchmark MOFs. Moreover, comparing the  $Q_{st}$  of CO<sub>2</sub> with other MOFs, ZU-610a showed the lowest  $Q_{st}$  of 27.3 kJ/mol, indicating its extremely low regeneration energy. Kinetic studies of MOFs for CO<sub>2</sub>/C<sub>2</sub>H<sub>2</sub> separation

have been less reported, and this research offered recommendations for the design of MOFs for separation systems with comparable molecular dimensions.

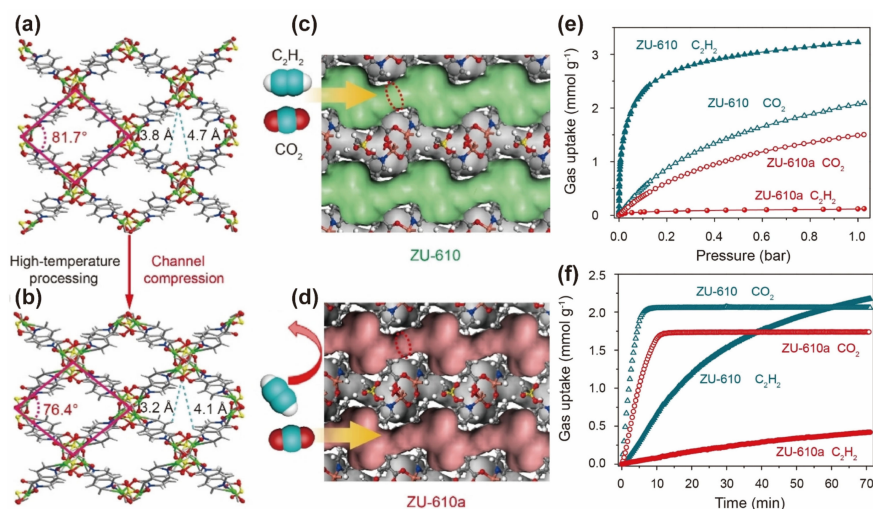


**Figure 10.** (a,b) The structures and rhombic channel of ZU-610 (a) and ZU-610a (b). (c,d) The 1D channel of ZU-610 (c) and ZU-610a (d). (e) Sorption isotherms of  $C_2H_2$  and  $CO_2$ . (f) Gas adsorption of  $C_2H_2$  and  $CO_2$  versus time at 298 K, 1 bar. Reproduced with permission from Cui et al., *Angewandte Chemie International Edition*; published by John Wiley and Sons, 2022 [81].

Overall,  $C_2H_2$  is the most similar substance to  $CO_2$  in terms of physical properties. The challenge of directly capturing  $CO_2$  instead of  $C_2H_2$  from  $CO_2/C_2H_2$  is to avoid stronger electrostatic interactions between  $C_2H_2$  and the adsorbent. The separation by exploiting the flexibility of MOFs is fascinating but less predictable, making it difficult to develop design principles. Optimizing the pore chemistry through different electrostatic interactions or thermodynamic affinity will be more opportune.

#### 4. $CO_2$ -Selective Capture from Other Binary Light Hydrocarbon Mixtures

High-purity ethylene ( $C_2H_4$ ) and ethane ( $C_2H_6$ ) are important raw materials to produce plastics, rubber and other industrial chemicals but always contain contaminants such as  $CO_2$ , which is corrosive to gas pipelines and can affect the conversion of products. In addition,  $C_2H_4$  and  $C_2H_6$  can form maximum pressure azeotrope with  $CO_2$ , which is a barrier to  $CO_2$  removal by distillation [88,89]. Compared to  $C_2H_2$ , however, the kinetic diameter and polarizability of  $C_2H_4$  and  $C_2H_6$  differ more from  $CO_2$ ; therefore, many MOFs could exploit these differences for highly efficient separation.

Horike et al. reported an early study of a dense coordination framework [ $Zn(5NO_2-ip)(dpe)$ ] in 2012 [90]. [ $Zn(5NO_2-ip)(dpe)$ ] showed the inherent structural flexibility and  $CO_2$  preference over  $C_2H_4$  and  $C_2H_6$  under ambient conditions in single-component and mixed gas-flow experiments. For  $C_2H_6$ , the observed adsorption amount could be neglected (less than  $10\text{ cm}^3/\text{g}$  at 273 K, 8 bar). For  $C_2H_4$ , the adsorption isotherm represented a gate-opening behavior. At 298 K, the pressure at which adsorption begins was 720 kPa, whereas the total uptake was only  $32\text{ mL}/\text{g}$  at 800 kPa. For  $CO_2$ , however, the adsorption capacity reached  $31\text{ mL}/\text{g}$  at 298 K and 101 kPa with a type I isotherm. Breakthrough curves were measured for a mixture of  $C_2H_4/CO_2$  (80/20,  $v/v$ ) at 298 K, with outlet  $C_2H_4$  purity of almost 100%, exhibiting the significant separation property of  $CO_2$  over  $C_2H_4$ .

In a subsequent study, a family of rare earth MOFs (named RE-PCP) were designed with various flexibility from an acrylamide-modified ligand for  $CO_2/C_2H_6$  and  $CO_2/C_2H_4$  separation [88]. At 195 K, Y-PCP and Ho-PCP showed fully reversible type I isotherms for  $CO_2$  and  $C_2H_4$  with higher  $CO_2$  capacity than  $C_2H_4$ . However, the adsorption of  $CO_2$  in La-PCP showed a “gate opening” phenomenon, and at around 80 kPa, the second uptake occurred. In contrast, even at pressures up to 100 kPa, there was almost no absorption for

C<sub>2</sub>H<sub>4</sub> or C<sub>2</sub>H<sub>6</sub> in La-PCP. The total CO<sub>2</sub> uptake by La-PCP was approximately 34 mL/g at 273 K, 150 kPa, whereas the adsorption of C<sub>2</sub>H<sub>4</sub> and C<sub>2</sub>H<sub>6</sub> was almost absent before 150 kPa, indicating that La-PCP is a potential candidate for CO<sub>2</sub> capture from CO<sub>2</sub>/C<sub>2</sub>H<sub>4</sub> and CO<sub>2</sub>/C<sub>2</sub>H<sub>6</sub> mixtures.

Qc-5-Cu has been demonstrated to be efficient in CO<sub>2</sub>/C<sub>2</sub>H<sub>4</sub> separation, with high thermal and water stability [91]. The pore diameter of Qc-5-Cu was estimated to be approximately 3.3 Å, which is similar to the molecular dimensions of CO<sub>2</sub> (3.3 Å) but smaller than those of C<sub>2</sub>H<sub>4</sub> (4.16 Å). Thus, Qc-5-Cu could molecularly sieve CO<sub>2</sub> from C<sub>2</sub>H<sub>4</sub> to achieve a high selectivity of 39.95 for a CO<sub>2</sub>/C<sub>2</sub>H<sub>4</sub> (*v/v*, 1:99) mixture. The saturation capacity of CO<sub>2</sub> also reached 2.48 mmol/g. The *Q*<sub>st</sub> value for CO<sub>2</sub> and C<sub>2</sub>H<sub>4</sub> was calculated to be 36.2 kJ/mol and 23.1 kJ/mol, respectively, indicating the higher CO<sub>2</sub> adsorption intensity. However, these results are considerably lower than those of MOFs with OMSs, leading to lower regeneration energy costs.

[Co(pysa)(H<sub>2</sub>O)]<sub>n</sub> (YAU-7) was synthesized from H<sub>2</sub>pysa (2-(pyrid-4'-yl)-benzimidazole-5-carboxylic acid) with superior separation performance for CO<sub>2</sub>, C<sub>2</sub>H<sub>2</sub> and C<sub>2</sub>H<sub>4</sub> [92]. Among these four gases, YAU-7 was found to be most favorable for the adsorption of CO<sub>2</sub>. Importantly, YAU-7 had a high selectivity of 36.8, 80.7 and 31.6 for CO<sub>2</sub>/CH<sub>4</sub>, CO<sub>2</sub>/C<sub>2</sub>H<sub>2</sub> and CO<sub>2</sub>/C<sub>2</sub>H<sub>4</sub> (*v/v*, 50/50) mixtures at 298 K and 100 kPa, respectively. However, its CO<sub>2</sub> capacity was only 1.53 mmol/g under 298 K, 100 kPa.

The SU-101(M) series MOFs, which comprise Bi, In, Ga and Al, have a small pore size of approximately 6.8 Å and an abundance of carbonyl oxygen atoms in the channel, which could act as Lewis basic sites to bind acidic CO<sub>2</sub> [82]. Each metal center in SU-101(M) was coordinated to one coordinated H<sub>2</sub>O molecule. Compared to the fully activated phase SU-101(M)-a, which did not contain coordinated H<sub>2</sub>O, the presence of coordinated H<sub>2</sub>O in SU-101(M) strengthened the interaction between the C atom in CO<sub>2</sub> and carbonyl O with more electrons, whereas it weakened interactions with both C<sub>2</sub>H<sub>2</sub> and C<sub>2</sub>H<sub>4</sub>. Therefore, SU-101(M) showed a high CO<sub>2</sub> capacity of 40.2–53.7 mL/g (1.79–2.4 mmol/g) and a high selectivity of 5.5–15.5. The *Q*<sub>st</sub> values of CO<sub>2</sub> were also obviously larger than those of C<sub>2</sub>H<sub>2</sub> and C<sub>2</sub>H<sub>4</sub>.

The kinetic diameters and polarizabilities of C<sub>2</sub>H<sub>4</sub> and C<sub>2</sub>H<sub>6</sub> differ more from those of CO<sub>2</sub> compared to C<sub>2</sub>H<sub>2</sub>, which is why many MOFs can efficiently separate CO<sub>2</sub> based on these differences. Future research should focus on further increasing the adsorption capacity of CO<sub>2</sub> and reducing the energy consumption for regeneration. Moreover, the efficient capture of CO<sub>2</sub> from multiple C<sub>1</sub>-C<sub>2</sub> mixtures is also very attractive.

In addition to C<sub>1</sub> and C<sub>2</sub> components, gaseous light hydrocarbons also include C<sub>3</sub> and C<sub>4</sub> components, such as propylene (C<sub>3</sub>H<sub>6</sub>), propane (C<sub>3</sub>H<sub>8</sub>), butene (C<sub>4</sub>H<sub>8</sub>), etc. Their physical properties differ more significantly from those of CO<sub>2</sub>, which are easier to separate. Therefore, CO<sub>2</sub> capture from C<sub>3</sub> and C<sub>4</sub> mixtures has not attracted much attention from researchers and is outside the scope of this review.

## 5. CO<sub>2</sub>-Selective Capture from Multicomponent Light Hydrocarbon Mixtures

Porous materials capable of recognizing CO<sub>2</sub> with high selectivity and specificity from a more complex system have always been a goal pursued by researchers; therefore, attention needs to be paid to the development of MOFs that capture CO<sub>2</sub> from multiple components.

Some MOFs with CO<sub>2</sub>/C<sub>2</sub>H<sub>2</sub> inverse selectivity mentioned in Section 2 can also exhibit a higher capacity for CO<sub>2</sub> than some other light hydrocarbons. For instance, Cd-NP was reported to selectively adsorb CO<sub>2</sub> over C<sub>2</sub>H<sub>2</sub> through optimization of the ESP of the pore surface; moreover, with a narrow pore size of 3.2 Å, it did not adsorb larger molecules at all, such as C<sub>2</sub>H<sub>4</sub> and C<sub>2</sub>H<sub>6</sub> [75]. The presence of coordinated H<sub>2</sub>O in SU-101(M) strengthened the CO<sub>2</sub> adsorption but reduced both C<sub>2</sub>H<sub>2</sub> and C<sub>2</sub>H<sub>4</sub> adsorption. Taking SU-101(Al) as an example, the equimolar CO<sub>2</sub>/C<sub>2</sub>H<sub>2</sub> and CO<sub>2</sub>/C<sub>2</sub>H<sub>4</sub> selectivities were 15.5 and 8.3 at 298 K 100 kPa, respectively, showing the potential of SU-101(Al) for CO<sub>2</sub> capture from C<sub>2</sub>H<sub>2</sub> and C<sub>2</sub>H<sub>4</sub>.

[Zn(odip)<sub>0.5</sub>(bpe)<sub>0.5</sub>] is a flexible MOF with a gate-opening effect for efficient purification of C<sub>1</sub>-C<sub>2</sub> hydrocarbons and CO<sub>2</sub> capture [54]. At 298 K, a gate-opening behavior for CO<sub>2</sub> was clearly observed. The adsorption of CO<sub>2</sub> first rapidly reached 55.0 mL/g at 20.7 kPa and then suddenly increased to 118.7 mL/g (5.30 mmol/g) until 100 kPa. For C<sub>1</sub> and C<sub>2</sub> hydrocarbons, no clear gate-adsorption behaviors occurred, but lower adsorption was observed at all temperatures. Owing to the gate-opening behavior for CO<sub>2</sub>, the selectivities for equimolar mixtures of [Zn(odip)<sub>0.5</sub>(bpe)<sub>0.5</sub>] were 376.0 for CO<sub>2</sub>/CH<sub>4</sub>, 13.2 for CO<sub>2</sub>/C<sub>2</sub>H<sub>2</sub>, 26.2 for CO<sub>2</sub>/C<sub>2</sub>H<sub>4</sub> and 27.9 for CO<sub>2</sub>/C<sub>2</sub>H<sub>6</sub> at 298 K, 100 kPa.

However, practical multicomponent breakthrough experiments to demonstrate separation performance are lacking in these studies. Qazvini et al. provided MUF-16-M (M = Co, Mn, Ni)-type MOFs from 5-aminoisophthalic acid (H<sub>2</sub>aip) [51]. The pore chemistry of MUF-16-M was precisely designed with complementary size (3.6 × 7.6 Å) and electrostatic potential to CO<sub>2</sub>. Single-crystal XRD and DFT calculations indicated that the O atoms of CO<sub>2</sub> could form N-H···O and C-H···O hydrogen bonds with the -NH<sub>2</sub> and phenyl groups, whereas the electropositive C atom contacted the O atom from the two uncoordinated carboxyl groups. The adsorption of N<sub>2</sub>O with similar size and electrostatic distribution on MUF-16 confirmed this binding mode. The uptake capacities of MUF-16 were 47.78 mL/g for CO<sub>2</sub>, 1.20 mL/g for CH<sub>4</sub>, 3.99 mL/g for C<sub>2</sub>H<sub>2</sub>, 3.17 mL/g for C<sub>2</sub>H<sub>4</sub>, 3.06 mL/g for C<sub>2</sub>H<sub>6</sub>, 5.35 mL/g for C<sub>3</sub>H<sub>6</sub> and 4.82 mL/g for C<sub>3</sub>H<sub>8</sub>. For equimolar CO<sub>2</sub>/CH<sub>4</sub> and CO<sub>2</sub>/C<sub>2</sub>H<sub>2</sub> mixtures, the selectivities were as high as 6690 and 510 at 293 K and 1 atm, respectively. MUF-16 successfully captured CO<sub>2</sub> from CO<sub>2</sub>/CH<sub>4</sub>/C<sub>2</sub>H<sub>6</sub>/C<sub>3</sub>H<sub>8</sub> (15/80/4/1) mixtures at 1.1 bar in a breakthrough experiment with steep elution profiles (Figure 11). On account of these features, MUF-16 is a promising physical adsorbent for direct capture of CO<sub>2</sub> from multicomponent light hydrocarbon mixtures.

The study of CO<sub>2</sub> capture from multiple hydrocarbon mixtures is still at the beginning stage, and it is expected to be a hot research topic, as it is very difficult but urgently needed. Finely tuning the pore chemistry or developing flexible MOFs with gate-opening behavior for CO<sub>2</sub> represent very promising strategies. We expect more valuable research to explore how to specifically recognize CO<sub>2</sub> and extend it to other CO<sub>2</sub> mixture systems.

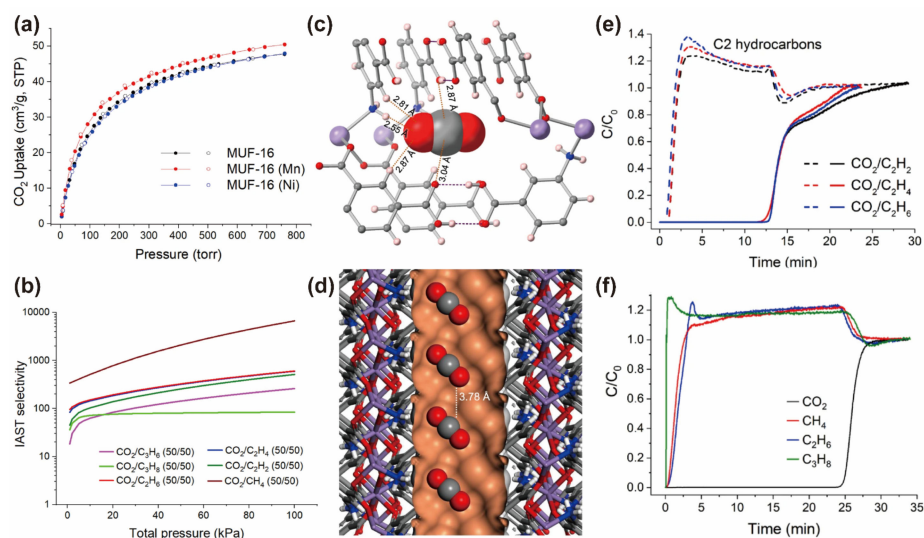


**Figure 11.** (a) The adsorption/desorption isotherms for CO<sub>2</sub> at 293 K. (b) IAST selectivities of MUF-16 for different mixtures (50/50) at 293 K. (c,d) The adsorption sites (c) and arrangement (d) of adsorbed CO<sub>2</sub> molecules in MUF-16(Mn). Color codes: Mn, lilac; N, blue; O, red; C, gray; H, light pink or white; pore surface, orange. (e,f) Breakthrough experiment curves for CO<sub>2</sub>/C<sub>2</sub> (50/50) (e) and CO<sub>2</sub>/CH<sub>4</sub>/C<sub>2</sub>H<sub>6</sub>/C<sub>3</sub>H<sub>8</sub> (15/80/4/1) (f) at 293 K and 1.1 bar for MUF-16. Reproduced with permission from Qazvini et al., Nature Communications; published by Springer Nature, 2021 [51].

## 6. Outlook

Capturing CO<sub>2</sub> from various gas mixtures is a necessary prerequisite for subsequent CO<sub>2</sub> reduction, conversion, utilization or storage technologies. From this perspective, the issue of CO<sub>2</sub> capture has been recognized as one of the major challenges of the 21st century. With further understanding of the pore chemistry, structural flexibility and host-guest interaction of MOFs, additional progress has been made in the field of CO<sub>2</sub> capture from light hydrocarbon mixtures. In situ characterization and theoretical computational studies have revealed the mechanisms of selective CO<sub>2</sub> recognition behavior at the molecular level, providing an important impetus for the development of MOFs.

Although MOF chemistry has recently made considerable progress, there are several aspects of practical applications that remain challenging and deserve further exploration in the future:

- (1) Elimination of the trade-off between CO<sub>2</sub> uptake capacity and selectivity. This problem is more evident in CO<sub>2</sub> capture from CO<sub>2</sub>/C<sub>2</sub>H<sub>2</sub> mixtures, as they are extremely close in nature. To develop optimal MOFs combining high CO<sub>2</sub> selectivity and high capacity, in the future, researchers should focus on (a) designing flexible MOFs that can transform structures to accommodate target gas to substantially improve selectivity; (b) hyperfine control of pore size, shape and environment through reticular chemistry or crystal engineering strategies; and (c) developing MOF composites or grading combination strategies to compensate for the shortcomings of individual pristine MOFs.
- (2) CO<sub>2</sub>-selective capture at trace concentrations. The CO<sub>2</sub>/hydrocarbon ratios used for experiments in most studies are 1/1, 1/2 or 1/9, whereas the initial concentration of CO<sub>2</sub> in real hydrocarbon mixtures is typically much lower (<5%). It is extremely challenging to maintain superior selective adsorption for CO<sub>2</sub> at such low concentrations. In this regard, flexible MOFs with gate-opening effects for CO<sub>2</sub> at low pressure are highly promising.
- (3) CO<sub>2</sub> selective adsorption from multicomponent hydrocarbon mixtures. Porous materials capable of recognizing CO<sub>2</sub> in more complex systems with high selectivity and specificity are extremely challenging but sought-after for material design. A grading combination of multiple MOFs or integration of pores with multiple properties into one MOF platform may be effective approaches.
- (4) Combination of desirable separation performance with broader performance for practical applications, such as high thermal/water/mechanical stability and low regeneration energy. Compared to conventional porous materials, MOF materials have more suitable ultra-microporous-level channels for CO<sub>2</sub> molecules, high designability and the potential to capture CO<sub>2</sub> from more complex systems. However, many MOFs are not as stable as porous carbon materials in terms of moisture stability and thermal stability. The introduction of open metal sites should be avoided, owing to their typically high activation temperature, regeneration energy consumption and poor water stability. An increasing number of researchers are employing strategies such as the construction of robust coordination geometries to build stable MOF materials.
- (5) Further reduction in economic and energy costs (from precursors, solvents, synthesis temperatures, activation conditions, etc.). Unaffordable raw materials and severe synthesis or activation conditions have become one of the most challenging issues in scaling MOFs up for practical applications.
- (6) Large-scale synthesis and industrialization. Taking technology from the laboratory to industrialization is always a challenge. A good adsorbent material should be synthesized on a large scale with high purity; however, this is rarely achieved in MOF studies. Making use of non-toxic metal ions, low-cost sustainable organic linkers and solvent-recoverable or solvent-free reactions may be beneficial in industrialization.
- (7) Introducing the design strategy of MOFs into other porous materials and other gas separation applications. For instance, in reticular chemistry, COFs and HOFs feature organic frameworks similar to that of MOFs and can therefore be developed by

introducing design strategies for MOFs. On the other hand, air is a complex gas mixture with a CO<sub>2</sub> concentration of only 0.04%. If MOFs for CO<sub>2</sub> capture from light hydrocarbons can be extended to direct CO<sub>2</sub> capture from air, considerable ecological and economic benefits can be realized.

Overall, it should be acknowledged that MOFs have shown tremendous potential for applications in the direct CO<sub>2</sub>-selective capture and purification of light hydrocarbons, owing to their high designability. Their implementation on a large scale offers the potential for significant environmental and economic benefits. Although there are still some challenging problems, we have confidence that with the persistent efforts of researchers working in this popular field, additional progress will be made in developing CO<sub>2</sub>-selective MOFs for light hydrocarbon purification.

**Author Contributions:** Conceptualization, Y.G. and H.H.; writing—original draft preparation, H.H.; writing—review and editing, Y.G., L.W., X.Z. and H.Z. All authors have read and agreed to the published version of the manuscript.

**Funding:** This research was funded by the National Key Research and Development Program of China (2022YFE0110500), the National Natural Science Foundation of China (21906120), the Shanghai Pujiang Program (NO. 21PJ1412600) and the Fundamental Research Funds for the Central Universities of China (22120220153).

**Institutional Review Board Statement:** Not applicable.

**Data Availability Statement:** Not applicable.

**Acknowledgments:** This work was supported by the National Key Research and Development Program of China (2022YFE0110500), the National Natural Science Foundation of China (21906120), the Shanghai Pujiang Program (NO.21PJ1412600) and the Fundamental Research Funds for the Central Universities of China (22120220153).

**Conflicts of Interest:** The authors declare no conflict of interest.

## References

1. Shi, X.; Xiao, H.; Azarabadi, H.; Song, J.; Wu, X.; Chen, X.; Lackner, K.S. Sorbents for the Direct Capture of CO<sub>2</sub> from Ambient Air. *Angew. Chem. Int. Ed.* **2020**, *59*, 6984–7006. [CrossRef] [PubMed]
2. Creamer, A.E.; Gao, B. Carbon-Based Adsorbents for Postcombustion CO<sub>2</sub> Capture: A Critical Review. *Environ. Sci. Technol.* **2016**, *50*, 7276–7289. [CrossRef] [PubMed]
3. Project, G.C. Annual CO<sub>2</sub> Emissions. Available online: <http://www.globalcarbonatlas.org/en/CO2-emissions> (accessed on 15 September 2022).
4. Pachauri, R.K.; Allen, M.R.; Barros, V.R.; Broome, J.; Cramer, W.; Christ, R.; Church, J.A.; Clarke, L.; Dahe, Q.; Dasgupta, P. *Climate Change 2014: Synthesis Report. Contribution of Working Groups I, II and III to the Fifth Assessment Report of the Intergovernmental Panel on Climate Change*; IPCC: Geneva, Switzerland, 2014.
5. Bui, M.; Adjiman, C.S.; Bardow, A.; Anthony, E.J.; Boston, A.; Brown, S.; Fennell, P.S.; Fuss, S.; Galindo, A.; Hackett, L.A.; et al. Carbon capture and storage (CCS): The way forward. *Energy Environ. Sci.* **2018**, *11*, 1062–1176. [CrossRef]
6. Yan, J.; Zhang, Z. Carbon Capture, Utilization and Storage (CCUS). *Appl. Energy* **2019**, *235*, 1289–1299. [CrossRef]
7. Sumida, K.; Rogow, D.L.; Mason, J.A.; McDonald, T.M.; Bloch, E.D.; Herm, Z.R.; Bae, T.-H.; Long, J.R. Carbon Dioxide Capture in Metal-Organic Frameworks. *Chem. Rev.* **2012**, *112*, 724–781. [CrossRef]
8. Sun, Y.; Tang, J.; Li, G.; Hua, Y.; Sun, Y.; Hu, S.; Wen, X. Adsorption, separation and regeneration of cation-exchanged X zeolites for LNG purification: Li<sup>+</sup>, K<sup>+</sup>, Mg<sup>2+</sup> and Ca<sup>2+</sup>. *Microporous Mesoporous Mater.* **2022**, *340*, 112032. [CrossRef]
9. Wang, S.; Li, X.; Wu, H.; Tian, Z.; Xin, Q.; He, G.; Peng, D.; Chen, S.; Yin, Y.; Jiang, Z.; et al. Advances in high permeability polymer-based membrane materials for CO<sub>2</sub> separations. *Energy Environ. Sci.* **2016**, *9*, 1863–1890. [CrossRef]
10. Pässler, P.; Hefner, W.; Buckl, K.; Meinass, H.; Meiswinkel, A.; Wernicke, H.-J.; Ebersberg, G.; Müller, R.; Bässler, J.; Behringer, H.; et al. Acetylene. In *Ullmann's Encyclopedia of Industrial Chemistry*; Wiley-VCH Verlag GmbH & Co. KGaA: Weinheim, Germany, 2011. [CrossRef]
11. Kitagawa, S. Porous Materials and the Age of Gas. *Angew. Chem. Int. Ed.* **2015**, *54*, 10686–10687. [CrossRef]
12. Göttlicher, G.; Pruschek, R. Comparison of CO<sub>2</sub> removal systems for fossil-fuelled power plant processes. *Energy Convers. Manage.* **1997**, *38*, S173–S178. [CrossRef]
13. Takht Ravanchi, M.; Sahebdehfar, S. Carbon dioxide capture and utilization in petrochemical industry: Potentials and challenges. *Appl. Petrochem. Res.* **2014**, *4*, 63–77. [CrossRef]
14. Rochelle, G.T. Amine Scrubbing for CO<sub>2</sub> Capture. *Science* **2009**, *325*, 1652–1654. [CrossRef]

15. Yang, R.T. *Gas Separation by Adsorption Processes*; Imperial College Press; World Scientific Publishing Co.: London, UK, 1997.
16. Zeng, H.; Qu, X.; Xu, D.; Luo, Y. Porous Adsorption Materials for Carbon Dioxide Capture in Industrial Flue Gas. *Front. Chem.* **2022**, *10*, 939701. [[CrossRef](#)]
17. Jahandar Lashaki, M.; Khiavi, S.; Sayari, A. Stability of amine-functionalized CO<sub>2</sub> adsorbents: A multifaceted puzzle. *Chem. Soc. Rev.* **2019**, *48*, 3320–3405. [[CrossRef](#)]
18. Sreenivasulu, B.; Sreedhar, I.; Suresh, P.; Raghavan, K.V. Development Trends in Porous Adsorbents for Carbon Capture. *Environ. Sci. Technol.* **2015**, *49*, 12641–12661. [[CrossRef](#)]
19. Silva, F.A.D.; Rodrigues, A.E. Propylene/propane separation by vacuum swing adsorption using 13X zeolite. *AIChE J.* **2001**, *47*, 341–357. [[CrossRef](#)]
20. Grande, C.A.; Poplow, F.; Rodrigues, A.E. Vacuum Pressure Swing Adsorption to Produce Polymer-Grade Propylene. *Sep. Sci. Technol.* **2010**, *45*, 1252–1259. [[CrossRef](#)]
21. Krishna, R. Methodologies for evaluation of metal-organic frameworks in separation applications. *RSC Adv.* **2015**, *5*, 52269–52295. [[CrossRef](#)]
22. Mersmann, A.; Fill, B.; Hartmann, R.; Maurer, S. The Potential of Energy Saving by Gas-Phase Adsorption Processes. *Chem. Eng. Technol.* **2000**, *23*, 937–944. [[CrossRef](#)]
23. Li, L.; Lin, R.-B.; Krishna, R.; Li, H.; Xiang, S.; Wu, H.; Li, J.; Zhou, W.; Chen, B. Ethane/ethylene separation in a metal-organic framework with iron-peroxo sites. *Science* **2018**, *362*, 443–446. [[CrossRef](#)]
24. Yang, L.; Qian, S.; Wang, X.; Cui, X.; Chen, B.; Xing, H. Energy-efficient separation alternatives: Metal-organic frameworks and membranes for hydrocarbon separation. *Chem. Soc. Rev.* **2020**, *49*, 5359–5406. [[CrossRef](#)]
25. Yang, S.-Q.; Hu, T.-L. Reverse-selective metal-organic framework materials for the efficient separation and purification of light hydrocarbons. *Coord. Chem. Rev.* **2022**, *468*, 214628. [[CrossRef](#)]
26. Burns, T.D.; Pai, K.N.; Subraveti, S.G.; Collins, S.P.; Krykunov, M.; Rajendran, A.; Woo, T.K. Prediction of MOF Performance in Vacuum Swing Adsorption Systems for Postcombustion CO<sub>2</sub> Capture Based on Integrated Molecular Simulations, Process Optimizations, and Machine Learning Models. *Environ. Sci. Technol.* **2020**, *54*, 4536–4544. [[CrossRef](#)] [[PubMed](#)]
27. Usman, M.; Iqbal, N.; Noor, T.; Zaman, N.; Asghar, A.; Abdelnaby, M.M.; Galadima, A.; Helal, A. Advanced Strategies in Metal-Organic Frameworks for CO<sub>2</sub> Capture and Separation. *Chem. Rec.* **2022**, *22*, e202100230. [[CrossRef](#)] [[PubMed](#)]
28. Liang, W.; Bhatt, P.M.; Shkurenko, A.; Adil, K.; Mouchaham, G.; Aggarwal, H.; Mallick, A.; Jamal, A.; Belmabkhout, Y.; Eddaoudi, M. A Tailor-Made Interpenetrated MOF with Exceptional Carbon-Capture Performance from Flue Gas. *Chem* **2019**, *5*, 950–963. [[CrossRef](#)]
29. Schneemann, A.; Bon, V.; Schwedler, I.; Senkovska, I.; Kaskel, S.; Fischer, R.A. Flexible metal-organic frameworks. *Chem. Soc. Rev.* **2014**, *43*, 6062–6096. [[CrossRef](#)]
30. Wang, Q.; Luo, J.; Zhong, Z.; Borgna, A. CO<sub>2</sub> capture by solid adsorbents and their applications: Current status and new trends. *Energy Environ. Sci.* **2011**, *4*, 42–55. [[CrossRef](#)]
31. Ding, M.; Flaig, R.W.; Jiang, H.-L.; Yaghi, O.M. Carbon capture and conversion using metal-organic frameworks and MOF-based materials. *Chem. Soc. Rev.* **2019**, *48*, 2783–2828. [[CrossRef](#)]
32. Sahoo, R.; Mondal, S.; Mukherjee, D.; Das, M.C. Metal-Organic Frameworks for CO<sub>2</sub> Separation from Flue and Biogas Mixtures. *Adv. Funct. Mater.* **2022**, *32*, 2207197. [[CrossRef](#)]
33. Bastin, L.; Barcia, P.S.; Hurtado, E.J.; Silva, J.A.C.; Rodrigues, A.E.; Chen, B. A Microporous Metal–Organic Framework for Separation of CO<sub>2</sub>/N<sub>2</sub> and CO<sub>2</sub>/CH<sub>4</sub> by Fixed-Bed Adsorption. *J. Phys. Chem. C* **2008**, *112*, 1575–1581. [[CrossRef](#)]
34. Barcia, P.S.; Bastin, L.; Hurtado, E.J.; Silva, J.A.C.; Rodrigues, A.E.; Chen, B. Single and Multicomponent Sorption of CO<sub>2</sub>, CH<sub>4</sub> and N<sub>2</sub> in a Microporous Metal-Organic Framework. *Sep. Sci. Technol.* **2008**, *43*, 3494–3521. [[CrossRef](#)]
35. Banerjee, R.; Furukawa, H.; Britt, D.; Knobler, C.; O’Keeffe, M.; Yaghi, O.M. Control of Pore Size and Functionality in Isoreticular Zeolitic Imidazolate Frameworks and their Carbon Dioxide Selective Capture Properties. *J. Am. Chem. Soc.* **2009**, *131*, 3875–3877. [[CrossRef](#)]
36. Bao, Z.; Yu, L.; Ren, Q.; Lu, X.; Deng, S. Adsorption of CO<sub>2</sub> and CH<sub>4</sub> on a magnesium-based metal organic framework. *J. Colloid Interface Sci.* **2011**, *353*, 549–556. [[CrossRef](#)]
37. Lin, R.-B.; Chen, D.; Lin, Y.-Y.; Zhang, J.-P.; Chen, X.-M. A Zeolite-Like Zinc Triazolate Framework with High Gas Adsorption and Separation Performance. *Inorg. Chem.* **2012**, *51*, 9950–9955. [[CrossRef](#)]
38. Burd, S.D.; Ma, S.; Perman, J.A.; Sikora, B.J.; Snurr, R.Q.; Thallapally, P.K.; Tian, J.; Wojtas, L.; Zaworotko, M.J. Highly Selective Carbon Dioxide Uptake by [Cu(bpy-n)<sub>2</sub>(SiF<sub>6</sub>)] (bpy-1 = 4,4’-Bipyridine; bpy-2 = 1,2-Bis(4-pyridyl)ethene). *J. Am. Chem. Soc.* **2012**, *134*, 3663–3666. [[CrossRef](#)]
39. Nugent, P.; Belmabkhout, Y.; Burd, S.D.; Cairns, A.J.; Luebke, R.; Forrest, K.; Pham, T.; Ma, S.; Space, B.; Wojtas, L.; et al. Porous materials with optimal adsorption thermodynamics and kinetics for CO<sub>2</sub> separation. *Nature* **2013**, *495*, 80–84. [[CrossRef](#)]
40. Du, L.; Lu, Z.; Zheng, K.; Wang, J.; Zheng, X.; Pan, Y.; You, X.; Bai, J. Fine-Tuning Pore Size by Shifting Coordination Sites of Ligands and Surface Polarization of Metal-Organic Frameworks To Sharply Enhance the Selectivity for CO<sub>2</sub>. *J. Am. Chem. Soc.* **2013**, *135*, 562–565. [[CrossRef](#)]
41. Yan, Q.; Lin, Y.; Kong, C.; Chen, L. Remarkable CO<sub>2</sub>/CH<sub>4</sub> selectivity and CO<sub>2</sub> adsorption capacity exhibited by polyamine-decorated metal-organic framework adsorbents. *Chem. Commun.* **2013**, *49*, 6873–6875. [[CrossRef](#)]

42. Chen, K.-J.; Madden, D.G.; Pham, T.; Forrest, K.A.; Kumar, A.; Yang, Q.-Y.; Xue, W.; Space, B.; Perry Iv, J.J.; Zhang, J.-P.; et al. Tuning Pore Size in Square-Lattice Coordination Networks for Size-Selective Sieving of CO<sub>2</sub>. *Angew. Chem. Int. Ed.* **2016**, *55*, 10268–10272. [[CrossRef](#)]
43. Jiang, M.; Li, B.; Cui, X.; Yang, Q.; Bao, Z.; Yang, Y.; Wu, H.; Zhou, W.; Chen, B.; Xing, H. Controlling Pore Shape and Size of Interpenetrated Anion-Pillared Ultramicroporous Materials Enables Molecular Sieving of CO<sub>2</sub> Combined with Ultrahigh Uptake Capacity. *ACS Appl. Mater. Interfaces* **2018**, *10*, 16628–16635. [[CrossRef](#)]
44. Jiang, J.; Lu, Z.; Zhang, M.; Duan, J.; Zhang, W.; Pan, Y.; Bai, J. Higher Symmetry Multinuclear Clusters of Metal–Organic Frameworks for Highly Selective CO<sub>2</sub> Capture. *J. Am. Chem. Soc.* **2018**, *140*, 17825–17829. [[CrossRef](#)]
45. Madden, D.G.; O’Nolan, D.; Chen, K.-J.; Hua, C.; Kumar, A.; Pham, T.; Forrest, K.A.; Space, B.; Perry, J.J.; Khraisheh, M.; et al. Highly selective CO<sub>2</sub> removal for one-step liquefied natural gas processing by physisorbents. *Chem. Commun.* **2019**, *55*, 3219–3222. [[CrossRef](#)] [[PubMed](#)]
46. Yang, L.; Cui, X.; Zhang, Y.; Wang, Q.; Zhang, Z.; Suo, X.; Xing, H. Anion Pillared Metal–Organic Framework Embedded with Molecular Rotors for Size-Selective Capture of CO<sub>2</sub> from CH<sub>4</sub> and N<sub>2</sub>. *ACS Sustain. Chem. Eng.* **2019**, *7*, 3138–3144. [[CrossRef](#)]
47. Mohan, M.; Essalhi, M.; Durette, D.; Rana, L.K.; Ayevide, F.K.; Maris, T.; Duong, A. A Rational Design of Microporous Nitrogen-Rich Lanthanide Metal–Organic Frameworks for CO<sub>2</sub>/CH<sub>4</sub> Separation. *ACS Appl. Mater. Interfaces* **2020**, *12*, 50619–50627. [[CrossRef](#)] [[PubMed](#)]
48. Gu, Y.-M.; Qi, H.-F.; Qadir, S.; Sun, T.-J.; Wei, R.; Zhao, S.-S.; Liu, X.-W.; Lai, Z.; Wang, S.-D. A Two-Dimensional Stacked Metal–Organic Framework for Ultra Highly-Efficient CO<sub>2</sub> Sieving. *Chem. Eng. J.* **2022**, *449*, 137768. [[CrossRef](#)]
49. Lin, R.-B.; Li, L.; Alsalmeh, A.; Chen, B. An Ultramicroporous Metal–Organic Framework for Sieving Separation of Carbon Dioxide from Methane. *Small Struct.* **2020**, *1*, 2000022. [[CrossRef](#)]
50. Hu, P.; Wang, H.; Xiong, C.; Liu, H.; Han, J.; Zhou, J.; Zhao, Z.; Wang, Y.; Ji, H. Probing the Node Chemistry of a Metal–Organic Framework to Achieve Ultrahigh Hydrophobicity and Highly Efficient CO<sub>2</sub>/CH<sub>4</sub> Separation. *ACS Sustain. Chem. Eng.* **2021**, *9*, 15897–15907. [[CrossRef](#)]
51. Qazvini, O.T.; Babarao, R.; Telfer, S.G. Selective capture of carbon dioxide from hydrocarbons using a metal-organic framework. *Nat. Commun.* **2021**, *12*, 197. [[CrossRef](#)]
52. Shi, Y.; Xie, Y.; Cui, H.; Alothman, Z.A.; Alduhaish, O.; Lin, R.-B.; Chen, B. An ultramicroporous metal–organic framework with dual functionalities for high sieving separation of CO<sub>2</sub> from CH<sub>4</sub> and N<sub>2</sub>. *Chem. Eng. J.* **2022**, *446*, 137101. [[CrossRef](#)]
53. Li, L.; He, J.; Xu, W.; Zhang, K.; Xing, T.; Li, Z.; Zhen, D.; Xiong, B.; Ge, Z.; Zhang, X.; et al. High CO<sub>2</sub> separation performance on a metal–organic framework composed of nano-cages lined with an ultra-high density of dual-side open metal sites. *Mater. Adv.* **2022**, *3*, 493–497. [[CrossRef](#)]
54. Ma, L.-N.; Wang, G.-D.; Hou, L.; Zhu, Z.; Wang, Y.-Y. Efficient One-Step Purification of C<sub>1</sub> and C<sub>2</sub> Hydrocarbons over CO<sub>2</sub> in a New CO<sub>2</sub>-Selective MOF with a Gate-Opening Effect. *ACS Appl. Mater. Interfaces* **2022**, *14*, 26858–26865. [[CrossRef](#)]
55. Lin, R.-B.; Li, L.; Zhou, H.-L.; Wu, H.; He, C.; Li, S.; Krishna, R.; Li, J.; Zhou, W.; Chen, B. Molecular sieving of ethylene from ethane using a rigid metal–organic framework. *Nat. Mater.* **2018**, *17*, 1128–1133. [[CrossRef](#)]
56. Navarro, J.A.R.; Barea, E.; Rodríguez-Diéguez, A.; Salas, J.M.; Ania, C.O.; Parra, J.B.; Masciocchi, N.; Galli, S.; Sironi, A. Guest-Induced Modification of a Magnetically Active Ultramicroporous, Gismondine-like, Copper(II) Coordination Network. *J. Am. Chem. Soc.* **2008**, *130*, 3978–3984. [[CrossRef](#)]
57. Ebadi Amooghini, A.; Sanaeepur, H.; Luque, R.; Garcia, H.; Chen, B. Fluorinated metal-organic frameworks for gas separation. *Chem. Soc. Rev.* **2022**, *51*, 7427–7508. [[CrossRef](#)]
58. Scott, H.S.; Shivanna, M.; Bajpai, A.; Madden, D.G.; Chen, K.-J.; Pham, T.; Forrest, K.A.; Hogan, A.; Space, B.; Perry Iv, J.J.; et al. Highly Selective Separation of C<sub>2</sub>H<sub>2</sub> from CO<sub>2</sub> by a New Dichromate-Based Hybrid Ultramicroporous Material. *ACS Appl. Mater. Interfaces* **2017**, *9*, 33395–33400. [[CrossRef](#)]
59. Gao, J.; Qian, X.; Lin, R.-B.; Krishna, R.; Wu, H.; Zhou, W.; Chen, B. Mixed Metal–Organic Framework with Multiple Binding Sites for Efficient C<sub>2</sub>H<sub>2</sub>/CO<sub>2</sub> Separation. *Angew. Chem. Int. Ed.* **2020**, *59*, 4396–4400. [[CrossRef](#)]
60. Pei, J.; Shao, K.; Wang, J.-X.; Wen, H.-M.; Yang, Y.; Cui, Y.; Krishna, R.; Li, B.; Qian, G. A Chemically Stable Hofmann-Type Metal–Organic Framework with Sandwich-Like Binding Sites for Benchmark Acetylene Capture. *Adv. Mater.* **2020**, *32*, 1908275. [[CrossRef](#)]
61. Yang, H.; Trieu, T.X.; Zhao, X.; Wang, Y.; Wang, Y.; Feng, P.; Bu, X. Lock-and-Key and Shape-Memory Effects in an Unconventional Synthetic Path to Magnesium Metal–Organic Frameworks. *Angew. Chem. Int. Ed.* **2019**, *58*, 11757–11762. [[CrossRef](#)]
62. Niu, Z.; Cui, X.; Pham, T.; Verma, G.; Lan, P.C.; Shan, C.; Xing, H.; Forrest, K.A.; Suepaul, S.; Space, B.; et al. A MOF-based Ultra-Strong Acetylene Nano-trap for Highly Efficient C<sub>2</sub>H<sub>2</sub>/CO<sub>2</sub> Separation. *Angew. Chem. Int. Ed.* **2021**, *60*, 5283–5288. [[CrossRef](#)]
63. Ye, Y.; Ma, Z.; Lin, R.-B.; Krishna, R.; Zhou, W.; Lin, Q.; Zhang, Z.; Xiang, S.; Chen, B. Pore Space Partition within a Metal–Organic Framework for Highly Efficient C<sub>2</sub>H<sub>2</sub>/CO<sub>2</sub> Separation. *J. Am. Chem. Soc.* **2019**, *141*, 4130–4136. [[CrossRef](#)]
64. Peng, Y.-L.; Pham, T.; Li, P.; Wang, T.; Chen, Y.; Chen, K.-J.; Forrest, K.A.; Space, B.; Cheng, P.; Zaworotko, M.J.; et al. Robust Ultramicroporous Metal–Organic Frameworks with Benchmark Affinity for Acetylene. *Angew. Chem. Int. Ed.* **2018**, *57*, 10971–10975. [[CrossRef](#)]

65. Lee, J.; Chuah, C.Y.; Kim, J.; Kim, Y.; Ko, N.; Seo, Y.; Kim, K.; Bae, T.H.; Lee, E. Separation of Acetylene from Carbon Dioxide and Ethylene by a Water-Stable Microporous Metal–Organic Framework with Aligned Imidazolium Groups inside the Channels. *Angew. Chem. Int. Ed.* **2018**, *57*, 7869–7873. [[CrossRef](#)] [[PubMed](#)]
66. Luo, F.; Yan, C.; Dang, L.; Krishna, R.; Zhou, W.; Wu, H.; Dong, X.; Han, Y.; Hu, T.-L.; O’Keeffe, M.; et al. UTSA-74: A MOF-74 Isomer with Two Accessible Binding Sites per Metal Center for Highly Selective Gas Separation. *J. Am. Chem. Soc.* **2016**, *138*, 5678–5684. [[CrossRef](#)] [[PubMed](#)]
67. Eguchi, R.; Uchida, S.; Mizuno, N. Inverse and High CO<sub>2</sub>/C<sub>2</sub>H<sub>2</sub> Sorption Selectivity in Flexible Organic–Inorganic Ionic Crystals. *Angew. Chem. Int. Ed.* **2012**, *51*, 1635–1639. [[CrossRef](#)] [[PubMed](#)]
68. Ma, B.; Li, D.; Zhu, Q.; Li, Y.; Ueda, W.; Zhang, Z. A Zeolitic Octahedral Metal Oxide with Ultra-Microporosity for Inverse CO<sub>2</sub>/C<sub>2</sub>H<sub>2</sub> Separation at High Temperature and Humidity. *Angew. Chem. Int. Ed.* **2022**, *61*, e202209121. [[CrossRef](#)] [[PubMed](#)]
69. Yang, W.; Davies, A.J.; Lin, X.; Suyetin, M.; Matsuda, R.; Blake, A.J.; Wilson, C.; Lewis, W.; Parker, J.E.; Tang, C.C.; et al. Selective CO<sub>2</sub> uptake and inverse CO<sub>2</sub>/C<sub>2</sub>H<sub>2</sub> selectivity in a dynamic bifunctional metal–organic framework. *Chem. Sci.* **2012**, *3*, 2993–2999. [[CrossRef](#)]
70. Foo, M.L.; Matsuda, R.; Hijikata, Y.; Krishna, R.; Sato, H.; Horike, S.; Hori, A.; Duan, J.; Sato, Y.; Kubota, Y.; et al. An Adsorbate Discriminatory Gate Effect in a Flexible Porous Coordination Polymer for Selective Adsorption of CO<sub>2</sub> over C<sub>2</sub>H<sub>2</sub>. *J. Am. Chem. Soc.* **2016**, *138*, 3022–3030. [[CrossRef](#)]
71. Chen, K.-J.; Scott, H.S.; Madden, D.G.; Pham, T.; Kumar, A.; Bajpai, A.; Lusi, M.; Forrest, K.A.; Space, B.; Perry, J.J.; et al. Benchmark C<sub>2</sub>H<sub>2</sub>/CO<sub>2</sub> and CO<sub>2</sub>/C<sub>2</sub>H<sub>2</sub> Separation by Two Closely Related Hybrid Ultramicroporous Materials. *Chem* **2016**, *1*, 753–765. [[CrossRef](#)]
72. Li, L.; Wang, J.; Zhang, Z.; Yang, Q.; Yang, Y.; Su, B.; Bao, Z.; Ren, Q. Inverse Adsorption Separation of CO<sub>2</sub>/C<sub>2</sub>H<sub>2</sub> Mixture in Cyclodextrin-Based Metal–Organic Frameworks. *ACS Appl. Mater. Interfaces* **2019**, *11*, 2543–2550. [[CrossRef](#)]
73. Ma, D.; Li, Z.; Zhu, J.; Zhou, Y.; Chen, L.; Mai, X.; Liufu, M.; Wu, Y.; Li, Y. Inverse and highly selective separation of CO<sub>2</sub>/C<sub>2</sub>H<sub>2</sub> on a thulium–organic framework. *J. Mater. Chem. A* **2020**, *8*, 11933–11937. [[CrossRef](#)]
74. Gu, Y.; Zheng, J.-J.; Otake, K.-i.; Shivanna, M.; Sakaki, S.; Yoshino, H.; Ohba, M.; Kawaguchi, S.; Wang, Y.; Li, F.; et al. Host–Guest Interaction Modulation in Porous Coordination Polymers for Inverse Selective CO<sub>2</sub>/C<sub>2</sub>H<sub>2</sub> Separation. *Angew. Chem. Int. Ed.* **2021**, *60*, 11688–11694. [[CrossRef](#)]
75. Xie, Y.; Cui, H.; Wu, H.; Lin, R.-B.; Zhou, W.; Chen, B. Electrostatically Driven Selective Adsorption of Carbon Dioxide over Acetylene in an Ultramicroporous Material. *Angew. Chem. Int. Ed.* **2021**, *60*, 9604–9609. [[CrossRef](#)]
76. Zhang, Z.; Peh, S.B.; Krishna, R.; Kang, C.; Chai, K.; Wang, Y.; Shi, D.; Zhao, D. Optimal Pore Chemistry in an Ultramicroporous Metal–Organic Framework for Benchmark Inverse CO<sub>2</sub>/C<sub>2</sub>H<sub>2</sub> Separation. *Angew. Chem. Int. Ed.* **2021**, *60*, 17198–17204. [[CrossRef](#)]
77. Shi, Y.; Xie, Y.; Cui, H.; Ye, Y.; Wu, H.; Zhou, W.; Arman, H.; Lin, R.-B.; Chen, B. Highly Selective Adsorption of Carbon Dioxide over Acetylene in an Ultramicroporous Metal–Organic Framework. *Adv. Mater.* **2021**, *33*, 2105880. [[CrossRef](#)]
78. Li, X.-Y.; Song, Y.; Zhang, C.-X.; Zhao, C.-X.; He, C. Inverse CO<sub>2</sub>/C<sub>2</sub>H<sub>2</sub> separation in a pillared-layer framework featuring a chlorine-modified channel by quadrupole-moment sieving. *Sep. Purif. Technol.* **2021**, *279*, 119608. [[CrossRef](#)]
79. Cai, L.-Z.; Yao, Z.-Z.; Lin, S.-J.; Wang, M.-S.; Guo, G.-C. Photoinduced Electron-Transfer (PIET) Strategy for Selective Adsorption of CO<sub>2</sub> over C<sub>2</sub>H<sub>2</sub> in a MOF. *Angew. Chem. Int. Ed.* **2021**, *60*, 18223–18230. [[CrossRef](#)]
80. Choi, D.S.; Kim, D.W.; Kang, D.W.; Kang, M.; Chae, Y.S.; Hong, C.S. Highly selective CO<sub>2</sub> separation from a CO<sub>2</sub>/C<sub>2</sub>H<sub>2</sub> mixture using a diamine-appended metal–organic framework. *J. Mater. Chem. A* **2021**, *9*, 21424–21428. [[CrossRef](#)]
81. Cui, J.; Qiu, Z.; Yang, L.; Zhang, Z.; Cui, X.; Xing, H. Kinetic-Sieving of Carbon Dioxide from Acetylene through a Novel Sulfonic Ultramicroporous Material. *Angew. Chem. Int. Ed.* **2022**, *61*, e202208756. [[CrossRef](#)]
82. Hao, C.; Ren, H.; Zhu, H.; Chi, Y.; Zhao, W.; Liu, X.; Guo, W. CO<sub>2</sub>-favored metal-organic frameworks SU-101(M) (M = Bi, In, Ga, and Al) with inverse and high selectivity of CO<sub>2</sub> from C<sub>2</sub>H<sub>2</sub> and C<sub>2</sub>H<sub>4</sub>. *Sep. Purif. Technol.* **2022**, *290*, 120804. [[CrossRef](#)]
83. Gücüyener, C.; Van den Bergh, J.; Gascon, J.; Kapteijn, F. Ethane/Ethene Separation Turned on Its Head: Selective Ethane Adsorption on the Metal–Organic Framework ZIF-7 through a Gate-Opening Mechanism. *J. Am. Chem. Soc.* **2010**, *132*, 17704–17706. [[CrossRef](#)]
84. Böhme, U.; Barth, B.; Paula, C.; Kuhnt, A.; Schwieger, W.; Mundstock, A.; Caro, J.; Hartmann, M. Ethene/Ethane and Propene/Propane Separation via the Olefin and Paraffin Selective Metal–Organic Framework Adsorbents CPO-27 and ZIF-8. *Langmuir* **2013**, *29*, 8592–8600. [[CrossRef](#)]
85. Krause, S.; Hosono, N.; Kitagawa, S. Chemistry of Soft Porous Crystals: Structural Dynamics and Gas Adsorption Properties. *Angew. Chem. Int. Ed.* **2020**, *59*, 15325–15341. [[CrossRef](#)] [[PubMed](#)]
86. Gu, C.; Hosono, N.; Zheng, J.-J.; Sato, Y.; Kusaka, S.; Sakaki, S.; Kitagawa, S. Design and control of gas diffusion process in a nanoporous soft crystal. *Science* **2019**, *363*, 387–391. [[CrossRef](#)] [[PubMed](#)]
87. Behera, N.; Duan, J.; Jin, W.; Kitagawa, S. The chemistry and applications of flexible porous coordination polymers. *EnergyChem* **2021**, *3*, 100067. [[CrossRef](#)]
88. Duan, J.; Higuchi, M.; Foo, M.L.; Horike, S.; Rao, K.P.; Kitagawa, S. A Family of Rare Earth Porous Coordination Polymers with Different Flexibility for CO<sub>2</sub>/C<sub>2</sub>H<sub>4</sub> and CO<sub>2</sub>/C<sub>2</sub>H<sub>6</sub> Separation. *Inorg. Chem.* **2013**, *52*, 8244–8249. [[CrossRef](#)]
89. Kelman, S.; Lin, H.; Sanders, E.S.; Freeman, B.D. CO<sub>2</sub>/C<sub>2</sub>H<sub>6</sub> separation using solubility selective membranes. *J. Membr. Sci.* **2007**, *305*, 57–68. [[CrossRef](#)]

90. Horike, S.; Kishida, K.; Watanabe, Y.; Inubushi, Y.; Umeyama, D.; Sugimoto, M.; Fukushima, T.; Inukai, M.; Kitagawa, S. Dense Coordination Network Capable of Selective CO<sub>2</sub> Capture from C<sub>1</sub> and C<sub>2</sub> Hydrocarbons. *J. Am. Chem. Soc.* **2012**, *134*, 9852–9855. [[CrossRef](#)]
91. He, T.; Xiao, Y.; Zhao, Q.; Zhou, M.; He, G. Ultramicroporous Metal–Organic Framework Qc-5-Cu for Highly Selective Adsorption of CO<sub>2</sub> from C<sub>2</sub>H<sub>4</sub> Stream. *Ind. Eng. Chem. Res.* **2020**, *59*, 3153–3161. [[CrossRef](#)]
92. Li, S.-Y.; Zhang, F.-F.; Wang, X.; He, M.-H.; Ding, Z.; Chen, M.; Hou, X.-Y.; Chen, X.-L.; Tang, L.; Yue, E.-L.; et al. Flexible ligands-dependent formation of a new column layered MOF possess 1D channel and effective separation performance for CO<sub>2</sub>. *J. Solid State Chem.* **2021**, *294*, 121896. [[CrossRef](#)]

**Disclaimer/Publisher’s Note:** The statements, opinions and data contained in all publications are solely those of the individual author(s) and contributor(s) and not of MDPI and/or the editor(s). MDPI and/or the editor(s) disclaim responsibility for any injury to people or property resulting from any ideas, methods, instructions or products referred to in the content.